The deubiquitinase Ubp3/Usp10 constrains glucose-mediated mitochondrial repression via phosphate budgeting

Vineeth Vengayil[1,2], Shreyas Niphadkar[1,2], Swagata Adhikary[1,2], Sriram Varahan[1], Sunil Laxman[1]*

1. Institute for Stem Cell Science and Regenerative Medicine (DBT-inStem)
   GKVK Post Bellary Road
   Bangalore 560065
2. Manipal Academy of Higher Education, Manipal, Karnataka 576104, India

*correspondence: sunil@instem.res.in

Keywords: mitochondria, glycolysis, phosphate, deubiquitinase, Crabtree

Abstract

Many cells in high glucose repress mitochondrial respiration, as observed in the Crabtree and Warburg effects. Our understanding of biochemical constraints for mitochondrial activation is limited. Using a *Saccharomyces cerevisiae* screen, we identified the conserved deubiquitinase Ubp3 (Usp10), as necessary for mitochondrial repression. Ubp3 mutants have increased mitochondrial activity despite abundant glucose, along with decreased glycolytic enzymes, and a rewired glucose metabolic network with increased trehalose production. Utilizing *Δubp3* cells, along with orthogonal approaches, we establish that the high glycolytic flux in glucose continuously consumes free Pi. This restricts mitochondrial access to inorganic phosphate (Pi), and prevents mitochondrial activation. Contrastingly, rewired glucose metabolism with enhanced trehalose production and reduced GAPDH (as in *Δubp3* cells) restores Pi. This collectively results in increased mitochondrial Pi and derepression, while restricting mitochondrial Pi transport prevents activation. We therefore suggest that glycolytic-flux dependent intracellular Pi budgeting is a key constraint for mitochondrial repression.

Introduction

Rapidly proliferating cells have substantial metabolic and energy demands in order to increase biomass (1, 2). This includes a high ATP demand, obtained from cytosolic glycolysis or mitochondrial oxidative phosphorylation (OXPHOS), to fuel multiple reactions (3). Interestingly, many rapidly proliferating cells preferentially rely on ATP from glycolysis/fermentation over mitochondrial respiration even in oxygen-replete conditions, and is the well-known Warburg effect (4, 5). Many such cells repress mitochondrial processes in high glucose, termed glucose-mediated mitochondrial repression or the Crabtree effect (6, 7). This is observed in some tumors (5), neutrophils (8), activated macrophages (9), stem cells (10–12), and famously *Saccharomyces cerevisiae* (7). Numerous studies have identified signaling programs or regulators of glucose-mediated mitochondrial repression. However, biochemical programs and regulatory processes in biology evolve around key biochemical constraints (13). The biochemical constraints for mitochondrial repression remain unresolved (14, 15).

There are two hypotheses on the biochemical principles driving mitochondrial repression. The first proposes direct roles for glycolytic intermediates in driving mitochondrial respiration, by inhibiting specific mitochondrial outputs (16, 17). The second hypothesizes that a competition between glycolytic and mitochondrial processes for mutually required metabolites/co-factors such as pyruvate, ADP or inorganic phosphate (Pi) could determine the extent of mitochondrial repression (14, 15, 18). These are not all mutually exclusive, and a combination of these factors might dictate mitochondrial repression in high glucose. However, any hierarchies of importance are unclear (19), and experimental data for the necessary constraints for mitochondrial repression remains incomplete.

One approach to resolve this question has been to identify regulators of metabolic state under high glucose. Post-translational modifications (PTMs) regulated by signaling systems can regulate mitochondrial repression (20–22). Ubiquitination is a PTM that regulates global proteostasis (23, 24), but the roles of ubiquitination-dependent processes in regulating mitochondrial repression are poorly explored. Ubiquitination itself is determined by the balance between ubiquitination, and deubiquitinase (DUB) dependent deubiquitination (25). Little is known about the roles of DUBs in regulating metabolic states, making the DUBs interesting candidate regulators of mitochondrial repression.

63 In this study, using an *S. cerevisiae* DUB knock-out library-based screen, we identified
64 the evolutionarily conserved deubiquitinase Ubp3 (mammalian Usp10) as required for
65 mitochondrial repression in high glucose. Loss of Ubp3 resulted in mitochondrial activation,
66 along with a reduction in the glycolytic enzymes-phosphofructokinase 1 (Pfk1) and GAPDH
67 (Tdh2 and Tdh3). This consequently reroutes glucose flux and increases trehalose
68 biosynthesis. This metabolic rewiring increases Pi release from trehalose synthesis, and
69 decreases Pi consumption in glycolysis, to cumulatively increase Pi pools. Using *ubp3Δ* cells
70 along with independent analysis of wild-type cells, and isolated mitochondrial fractions, we
71 establish that glycolytic-flux dependent Pi allocations to mitochondria determines
72 mitochondrial activity. Through these data, we propose how intracellular Pi balance as
73 controlled by glycolytic flux, is a biochemical constraint for mitochondrial repression.

74 **Results**

75 **A deubiquitinase deletion screen identifies Ubp3 as a regulator of glucose-mediated**
76 **mitochondrial repression**

77 In cells such as *S. cerevisiae*, high glucose represses mitochondrial activity as well as
78 OXPHOS-dependent ATP synthesis (7, 26) (illustrated in Figure 1A). Our initial objective was
79 to identify proteostasis regulators of glucose-mediated mitochondrial repression. We
80 generated and used a deubiquitinase (DUB) deletion strain library of *S. cerevisiae* (Figure 1-
81 figure supplement 1A), to unbiasedly identify regulators of mitochondrial repression by
82 measuring the fluorescence intensity of a potentiometric dye Mitotracker CMXRos (illustrated
83 in Figure 1B). Using this screen, we identified DUB mutants with altered mitochondrial
84 membrane potential (Figure 1C, Figure 1-figure supplement 1 A). Note: WT cells in a
85 respiratory medium (2% ethanol) were used as a control to estimate maximum mitotracker
86 fluorescence intensity (Figure 1-figure supplement 1B).

87 A prominent 'hit' was the evolutionarily conserved deubiquitinase Ubp3 (Figure 1C),
88 (homologous to mammalian Usp10) (Figure 1-figure supplement 1D). Due to its high degree
89 of conservation across eukaryotes (Figure 1-figure supplement 1D) as well as putative roles in
90 metabolism or mitochondrial function (27–29), we focused our further attention on this DUB.
91 Cells lacking Ubp3 showed an ~1.5-fold increase in mitotracker fluorescence (Figure 1C, Figure

92 1-figure supplement 1A, C). Cells with catalyticaly inactive Ubp3 (Ubp3^{C469A}), showed
93 increased mitochondrial potential comparable to *ubp3Δ* (Figure 1D). This data confirmed that
94 Ubp3 catalytic activity of is required to fully repress mitochondrial activity under high glucose.
95 The catalytic site mutation did not affect steady-state Ubp3 levels (Figure 1-figure supplement
96 1E).

97 Next, to assess the requirement of Ubp3 for mitochondrial function, we quantified the
98 electron transport chain (ETC) complex IV subunit Cox2 (30)(Figure 1E). *ubp3Δ* had higher
99 Cox2 than WT (Figure 1E). As a control, we estimated total mitochondrial content in WT and
100 *ubp3Δ* cells, using either estimates of the structural protein Tom70, or measuring the
101 fluorescence-intensity in strains engineered with mitochondrial targeted mNeonGreen (31).
102 There was no increase in the total mitochondrial volume (estimated by measuring the
103 intensity of mitochondria targeted mNeon green) (Figure 1-figure supplement 1F) or
104 mitochondrial outer membrane protein Tom70 (Figure 1-figure supplement 1G). This suggests
105 that the increased Cox2 is not merely because of higher total mitochondrial content. We next
106 measured the basal oxygen consumption rate (OCR) of *ubp3Δ*, and basal OCR was higher in
107 *ubp3Δ*, indicating higher respiration (Figure 1F).

108 Next, we asked if mitochondrial ATP synthesis was higher in *ubp3Δ*. The total ATP
109 levels in WT and *ubp3Δ* were comparable (Figure 1G). However, upon treatment with the ETC
110 complex IV inhibitor sodium azide, ATP levels in WT were higher than *ubp3Δ*, contributing to
111 ~60% of the total ATP (Figure 1H). In contrast, the ATP levels in *ubp3Δ* after sodium azide
112 treatment were ~ 40% of the total ATP (Figure 1H). These data suggest a higher contribution
113 of mitochondrial ATP synthesis towards the total ATP pool in *ubp3Δ*.

114 We next asked if *ubp3Δ* required higher mitochondrial activity for growth, using a
115 series of mitochondrial activity inhibitors and comparing relative growth. In high glucose, WT
116 cells show minimal growth inhibition in the presence of sodium azide, indicating lower
117 reliance on mitochondrial function (Figure 1I). Contrastingly, *ubp3Δ* or Ubp3^{C469A} show a
118 severe growth defect in the presence of the mitochondrial ETC complex inhbitors sodium
119 azide and oligomycin, and the mitochondrial OXPHOS uncoupler FCCP (Figure 1I, Figure 1-
120 figure supplement 1H). Additionally, the loss of Ubp3 in respiration defective cox2-62 cells
121 (32), or Rho0 cells (which lacks mitochondrial DNA) resulted in a severe growth defect (Figure

122 1-figure supplement 1I). Deletion of ATP synthase subunits Atp1 and Atp10 also results in a
123 severe growth defect in *ubp3Δ* compared to WT (Figure 1-figure supplement 1I). Together,
124 these results indicate that the loss of Ubp3 makes cells dependent on mitochondrial ATP
125 synthesis in high glucose.

126 Collectively these data show that in 2% glucose, *ubp3Δ* have high mitochondrial
127 activity, respiration, and rely on this mitochondrial function for ATP production and growth.
128 We therefore decided to use *ubp3Δ* cells to start delineating requirements for glucose-
129 mediated mitochondrial repression.

130

131 **Key glycolytic enzymes decrease and glucose flux is rerouted in *ubp3Δ* cells**

132 Glucose-6 phosphate (G6P) is the central node in glucose metabolism where carbon-
133 allocations are made towards distinct metabolic arms, primarily: glycolysis, the pentose
134 phosphate pathway (PPP), and trehalose biosynthesis (Figure 2A). We first compared
135 amounts of two key ('rate-controling') glycolytic enzymes - Phosphofructokinase 1 (Pfk1),
136 GAPDH isozymes (Tdh2, Tdh3) (3), along with the enolase isozymes (Eno1, Eno2) in WT and
137 *ubp3Δ* cells. Pfk1, Tdh2, and Tdh3 substantially decreased in *ubp3Δ* (but not Eno1 and Eno2)
138 (Figure 2B, Figure 2-figure supplement 1A). Since deubiquitinases can control protein
139 amounts by regulating proteasomal degradation, we asked if the decrease in Pfk1, Tdh2 and
140 Tdh3 in *ubp3Δ* is due to proteasomal degradation. To test this, we measured the levels of
141 these enzymes in *ubp3Δ* after treatement with proteasomal inhibitor MG132. We did not
142 observe any rescue in the levels of these enzymes in MG132 treated samples, suggesting that
143 the decreased levels of these enzymes were not due to increased proteasomal degradation
144 (Figure 2-figure supplement 1B). To further understand if these enzyme transcripts are
145 altered in *ubp3Δ*, we measured the mRNA levels of PFK1, TDH2 and TDH3 in WT, *ubp3Δ* and
146 $Ubp3^{C469A}$ cells. The transcripts of all the three genes in *ubp3Δ* and $Ubp3^{C469A}$ cells decreased
147 (Figure 2-figure supplement 1C), suggesting that Ubp3 regulates the transcripts of these
148 glycolytic enzyme genes. The reduction in the Pfk and GAPDH enzyme amounts was intriguing,
149 because the Pfk and GAPDH steps are critical in determining glycolytic flux (3, 33). A reduction
150 in these enzymes could therefore decrease glycolytic flux, and would reroute glucose (G6P)

151 allocations via mass action towards other branches of glucose metabolism, primarily the
152 pentose phosphate pathway as well as trehalose biosynthesis (Figure 2A). To assess this, we
153 first measured the steady-state levels of key glycolytic and pentose phosphate pathway (PPP)
154 intermediates, and trehalose in WT or *ubp3Δ* using targeted LC-MS/MS (Figure 2C, Figure 2-
155 figure supplement 1D). Glucose-6/fructose-6 phosphate (G6P/F6P) increased in *ubp3Δ* (Figure
156 2C). Concurrently, trehalose, and the PPP intermediates ribose 5-phosphate (R5P) and
157 sedoheptulose 7-phosphate (S7P), increased in *ubp3Δ* (Figure 2C).

158 Since steady-state metabolite amounts cannot separate production from utilization,
159 in order to unambiguously assess if glycolytic flux is reduced in *ubp3Δ* cells, we utilized a pulse
160 labeling of $^{13}C_6$ glucose, following which the label incorporation into glycolytic and other
161 intermediates was measured. Note that because glycolytic flux is very high in yeast, this
162 experiment would require rapid pulsing and extraction of metabolites in order to stay in a
163 linear range and avoid label saturation. We therefore established a very short time point of
164 label-addition, quenching and metabolite extraction post ^{13}C glucose pulse. Since flux
165 saturates/reaches steady-state in seconds, we first ensured that the label incorporation into
166 individual metabolites after the ^{13}C glucose pulse was in the linear range, and for early
167 glycolytic intermediates this was seconds after glucose addition. This new methodology is
168 extensively described in materials and methods, with required controls shown in Figure 2-
169 figure supplement 1F. WT and *ubp3Δ* cells were grown in high glucose, pulsed with $^{13}C_6$
170 glucose, and the relative ^{13}C label incorporation into glycolytic intermediates and trehalose
171 were measured, as shown in the schematic (Figure 2-figure supplement 1E). In *ubp3Δ,* ^{13}C
172 label incorporation into G6P/F6P as well as trehalose substantially increased (Figure 2D).
173 Contrastingly, ^{13}C label incorporation into glycolytic intermediates F1,6BP, G3P, 3PG and PEP
174 decreased, indicating decreased glycolytic flux (Figure 2D). We next measured ethanol
175 concentrations and production rates, as an additional output of relative glycolytic rates. We
176 observed decreased steady-state ethanol levels, as well as ethanol production rates in *ubp3Δ*
177 (Figure 2F).

178 Glycolysis-derived pyruvate is transported to mitochondria and fuels the TCA cycle.
179 Therefore, we asked if the decreased glycolytic rate result in a decrease in the TCA cycle flux
180 as well. To test this, we first measured the steady state levels of TCA cycle intermediates in
181 WT or *ubp3Δ* using targeted LC-MS/MS. We did not observe any significant change in the

182 levels of TCA cycle intermediates in *ubp3Δ,* except malate which showed a significant
183 decrease in *ubp3Δ* (Figure 2-figure supplement 2A). Next, in order to assess if TCA cycle flux
184 reduces in *ubp3Δ* cells, WT and *ubp3Δ* cells were grown in high glucose, pulsed with $^{13}C_6$
185 glucose, and the relative ^{13}C label incorporation into TCA cycle intermediates was measured,
186 as shown in the schematic (Figure 2-figure supplement 2B). The kinetics of ^{13}C label
187 incorporation in TCA cycle intermediates are shown in Figure 2-figure supplement 2C. We did
188 not observe any significant change in the relative ^{13}C label incorporation in TCA cycle
189 intermediates in *ubp3Δ.* Therefore, these data suggest that the decreased glycolytic flux in
190 *ubp3Δ* does not result in a decrease in TCA cycle flux. The increased respiration and
191 mitochondrial activity in *ubp3Δ* cells is therefore driven via other factors.

192 Collectively, these results reveal that that reduced Pfk1 and GAPDH (in *ubp3Δ*)
193 decrease glucose flux via glycolysis, which results in rewired glucose flux towards trehalose
194 biosynthesis and the PPP.

195

196 **Rerouted glucose flux results in phosphate (Pi) accumulation**

197 We therefore asked if the proteomic state, as observed in *ubp3Δ* cells, could provide
198 clues to explain the coupling between mitochondrial derepression and rerouted glucose flux.
199 A recent study by Isasa et al., had systematically quantified the changes in protein levels in
200 *ubp3Δ* cells (28). We therefore reanalyzed this extensive dataset, looking for changes in
201 proteins that would correlate with these metabolic processes. Notably, we observed
202 increased levels of proteins of the mitochondrial ETC and respiration, and decreased amounts
203 of glucose metabolizing enzymes in *ubp3Δ* (Figure 3A). Additionally, multiple proteins
204 involved in regulating phosphate (Pi) homeostasis were decreased in *ubp3Δ* (Figure 3A) (28).
205 We had recently uncovered a reciprocal coupling of Pi homeostasis with the different arms of
206 glucose metabolism, particularly trehalose biosynthesis (34, 35), and therefore wondered if a
207 glycolytic-flux dependent change in Pi homeostatsis had any role in mitochondrial respiration.
208 Our hypothesis was refined based on the reasoning given below.

209 One explanation for mitochondrial repression can be an internal competition for
210 shared metabolites/co-factors between (cytosolic) glycolytic and mitochondrial processes,

211 that mitochondria might not be sufficiently able to access (14, 18, 19). In this context, a
212 plausible role for inorganic phosphate (Pi) in regulating mitochondrial repression can be
213 hypothesized. Cytosolic glycolysis requires rapid, high consumption of net Pi (19, 36, 37), and
214 this could possibly limit the Pi that is continuously available for mitochondrial use (18, 38),
215 thereby repressing mitochondria. Contextually, the balance between reactions releasing vs
216 consuming Pi could explain changes in global Pi levels (35). A continuous hub of Pi
217 consumption is glycolysis. Here, GAPDH catalyzes G3P to 1,3BPG, converting ADP to ATP,
218 while concurrently consuming a molecule of Pi (37, 39). This Pi that goes into ATP will
219 subsequently be used for nucleotide biosynthesis, polyphosphate biosynthesis and protein
220 phosphorylation (35, 40). Therefore, we can surmise that in high glycolytic flux, the
221 production of ATP, nucleotides and polyphosphates is concurrent with Pi consumption (39,
222 41, 42). Could this reaction therefore limit cytosolic Pi for the mitochondria (as illustrated in
223 Figure 3B)? Notably, *ubp3Δ* have reduced GAPDH levels and decreased glycolytic flux. Second,
224 trehalose synthesis is a Pi releasing reaction, and a major source of free Pi that is critical for
225 Pi homeostasis (34, 37). Flux through this reaction is also substantially higher in *ubp3Δ*.
226 Therefore, these cells might have increased Pi release (via trehalose), coupled with
227 decreased Pi consumption (via decreased GAPDH). We therefore asked if total Pi increases in
228 *ubp3Δ* (Figure 3B)?

229 To test this, we directly assessed total Pi levels in *ubp3Δ* and WT. *ubp3Δ* cells had
230 higher Pi than WT, and this was comparable to Pi in WT grown in excess Pi (Figure 3C).
231 Similarly, Pi amounts also increased in Ubp3^{C469A} (Figure 3-figure supplement 1A). Therefore,
232 the loss of Ubp3 increases intracellular Pi levels. Next, we asked if *ubp3Δ* cells exhibit
233 signatures of a 'high Pi' state. *S. cerevisiae* maintains internal Pi balance by controlling the
234 expression of multiple genes collectively known as the Pho regulon (43). The Pho regulon is
235 induced under Pi limitation, and repressed during Pi sufficiency (34, 43). We assessed two
236 major Pho proteins (Pho84: a high-affinity membrane Pi transporter, and Pho12: an acid
237 phosphatase) in WT and *ubp3Δ* in high glucose. *ubp3Δ* cells have lower amounts of Pho84 and
238 Pho12 (Figure 3D). Further, upon shifting to low Pi for one hour, Pho84 and Pho12 increased
239 in *ubp3Δ*. These data suggest that reduced Pho84 and Pho12 amounts in *ubp3Δ* are because
240 of increased Pi, and not due to altered Pho regulon function itself (Figure 3D). These data

241 clarify earlier observations from *ubp3Δ* which noted reduced Pho proteins (28). Therefore,
242 *ubp3Δ* constitutively have higher Pi, and likely a consequent decrease in Pho proteins.

243 We next asked if the increased Pi in *ubp3Δ* is because of altered G6P allocations
244 towards different end-points, particularly trehalose synthesis, which can be a major node of
245 Pi restoration (34, 37). We assessed the contribution of increased trehalose synthesis towards
246 the high Pi in *ubp3Δ*, by estimating Pi levels in the absence of trehalose 6-phosphate
247 phosphatase (Tps2), which catalyzes the Pi-releasing step in trehalose synthesis. Notably, loss
248 of Tps2 in *ubp3Δ* decreased Pi (Figure 3E). There was no additive difference in Pi between
249 *tps2Δ* and *ubp3Δtps2Δ* (Figure 3E). As an added control, we assessed trehalose in WT and
250 *ubp3Δ* in the absence of Tps2, and found no difference (Figure 3-figure supplement
251 1B). Therefore, increasing G6P flux towards trehalose biosynthesis is a major source of the
252 increased Pi in *ubp3Δ*.

253 Since the major GAPDH isozymes, Tdh2 and Tdh3, are reduced in *ubp3Δ*, we directly
254 asked if reducing GAPDH can decrease Pi consumption and increase Pi. To assess this, we
255 generated *tdh2Δtdh3Δ* cells, which exhibit a growth defect, but are viable, permitting further
256 analysis. *tdh2Δtdh3Δ* had higher Pi in high glucose (Figure 3F). Expectedly, we observed a
257 decrease in ethanol in *tdh2Δtdh3Δ* (Figure 3-figure supplement 1C), along with an
258 accumulation of F1,6 BP and G3P, and decreased 3PG and PEP (Figure 3-figure supplement
259 1D). However, G6P and trehalose levels between WT and *tdh2Δtdh3Δ* were comparable
260 (Figure 3-figure supplement 1D, E). These data sugest that unlike in *ubp3Δ*, the increased Pi
261 in *tdh2Δtdh3Δ* comes mainly from decreased Pi consumption (GAPDH step). To further assess
262 the role of reduced glycolytic flux in increasing Pi (*ubp3Δ* and *tdh2Δtdh3Δ*), we measured the
263 Pi in these cells growing in a gluconeogenic medium – 2%, ethanol. In this scenario, the GAPDH
264 catalyzed reaction will be reversed, converting 1,3BPG to G3P, which should release and not
265 consume Pi. Compared to WT, the Pi levels decreased in *ubp3Δ* and *tdh2Δtdh3Δ* (Figure 3G),
266 suggesting that the changes in Pi in these mutants is driven by the relative change in Pi release
267 vs consumption.

268 These results collectively indicate that the combined effect of increased Pi release
269 coming from trehalose synthesis, and decreased Pi consumption from reduced GAPDH
270 increase Pi levels in *ubp3Δ*.

271

272 **Mitochondrial Pi availability correlates with mitochondrial activity in *ubp3Δ***

273 We therefore wondered if this observed Pi increase from the combined rewiring of
274 glucose metabolism resulted in more Pi becoming accessible to the mitochondria. This would
275 effectively result in Pi budgeting between cytosolic glycolysis and mitochondria based on the
276 relative flux in different arms of glucose metabolism, by increasing Pi availability for the
277 mitochondria (Figure 4A). To test if this were so, we first asked if the mitochondria in *ubp3Δ*
278 have increased Pi. Mitochondria were isolated by immunoprecipitation from WT and *ubp3Δ*,
279 the isolation efficiency was analyzed (Figure 4-figure supplement 1A), and relative Pi levels
280 compared. Pi levels were normalised to Idh1 (isocitrate dehydrogenase) in isolated
281 mitochondria, since Idh1 protein levels did not decrease in *ubp3Δ* (Figure 4-figure supplement
282 1B), and consistent with (28). Mitochondrial Pi was higher in *ubp3Δ* (Figure 4B). We next asked
283 if the increased mitochondrial activity in *ubp3Δ* is a consequence of high Pi. If this were so,
284 *tdh2Δtdh3Δ* should partially phenocopy *ubp3Δ* with respect to mitochondrial activity.
285 Consistently, *tdh2Δtdh3Δ* have higher mitotracker intensity as well as Cox2 levels compared
286 to WT (Figure 4-figure supplement 1C, Figure 4C). Also consistent with this, a high basal OCR
287 in *tdh2Δtdh3Δ* was observed (Figure 4D), together indicating high mitochondrial activity in
288 *tdh2Δtdh3Δ*, which is comparable to *ubp3Δ*.

289 We next asked if higher Pi is necessary to increase mitochondrial activity in *ubp3Δ* and
290 *tdh2Δtdh3Δ*. Since glycolysis is defective in *ubp3Δ* and *tdh2Δtdh3Δ*, it is necessary to
291 distinguish the effect of high Pi vs. only the effect of low glycolysis in activating mitochondria.
292 Logically, if decreased glycolysis (independent of Pi) is sufficient to activate mitochondria,
293 bringing down the Pi levels in *ubp3Δ* to that of WT should not affect mitochondrial activity.
294 Notably, *ubp3Δ* grown in low (1 mM) Pi have Pi levels similar to WT in standard (normal Pi)
295 medium (Figure 4-figure supplement 1D). *ubp3Δ* grown in low Pi also had decreased ethanol,
296 suggesting reduced glycolysis (Figure 4-figure supplement 1E). Therefore, we used this
297 condition to further understand the role of Pi in inducing mitochondrial activity. Mitotracker
298 fluorescence decreased in both *ubp3Δ* and *tdh2Δtdh3Δ* in low Pi (Figure 4-figure supplement
299 1F). Note: basal mitotracker fluorescence in WT also decreases in low Pi, which is consistent
300 with a required role of Pi for mitochondrial activity (Figure 4-figure supplement 1F). Similarly,

301 Cox2 levels were reduced in both *ubp3Δ* and *tdh2Δtdh3Δ* (Figure 4E). Consistent with both
302 reduced mitotracker intensity and Cox2 levels, basal OCR also decreased in both *ubp3Δ* and
303 *tdh2Δtdh3Δ* in low Pi (Figure 4F). As an additional control, we used Rho0 strains (which have
304 no mitochondrial DNA and therefore lack functional ETC) to compare basal OCR. The
305 expectation in these strains is that basal OCR will not change if Pi changes. Consistently, we
306 did not observe any significant difference in basal OCR in WT, *ubp3Δ* and *ubp3Δ* in low Pi in a
307 Rho0 strain background (which lacks mitochondrial DNA) (Figure 4-figure supplement 1G).
308 These data collectively suggest that high intracellular Pi is necessary to increase mitochondrial
309 activity in *ubp3Δ* and *tdh2Δtdh3Δ*.

310 Next, we asked how mitochondrial Pi transport regulates mitochondrial activity. Mir1
311 and Pic2 are mitochondrial Pi transporters, with Mir1 being the major Pi transporter (44, 45).
312 We first limited mitochondrial Pi availability in *ubp3Δ* by knocking-out *MIR1*. In *mir1Δ*, the
313 increased Cox2 observed in *ubp3Δ* was no longer observed (Figure 4G). Consistent with this,
314 we observed no further increase in the basal OCR in *mir1Δubp3Δ* compared to *mir1Δ* (Figure
315 4H). Furthermore, *mir1Δ* showed decreased Cox2 as well as basal OCR even in WT cells (Figure
316 4G, Figure 4H). These data together suggest that mitochondrial Pi transport is critical for
317 increasing mitochondrial activity in *ubp3Δ*, and in maintaining basal mitochondrial activity
318 even in high glucose.

319 As a control, no significant increase in Mir1 and Pic2 was observed in *ubp3Δ* (Figure 4-
320 figure supplement 1H), suggesting that *ubp3Δ* do not increase mitochondrial Pi by merely
321 increasing the Pi transporters, but rather by increasing available Pi pools.

322 Taken together, these data suggest the possibility that increased cytosolic Pi increases
323 the mitochondrial Pi pool, which increases mitochondrial activity. Decreasing mitochondrial
324 Pi by either reducing total Pi, or by reducing mitochondrial Pi transport decreases
325 mitochondrial activity.

326

327 **Mitochondrial Pi availability constrains mitochondrial activity under high glucose**

328 So far, these data suggest that the cytosolic Pi available for the mitochondria can
329 determine the extent of mitochondrial activity. Therefore, we further investigated if
330 mitochondrial Pi allocation was a necessary constraint for glucose-mediated mitochondrial
331 repression.

332 To test this, we first asked how important mitochondrial Pi transport was to switch to
333 increased respiration. In WT yeast, low glucose or glycolytic inhibition will result in increased
334 respiration (22). What happens therefore if we restrict mitochondrial Pi in this context? For
335 this, we measured the basal OCR in WT and *mir1Δ* after switching from high (2%) to low (0.1%)
336 glucose. We observed a significant increase in the basal OCR in WT but not in *mir1Δ* (Figure
337 5A). The alternate scenario is after glycolytic inhibition. We assessed the role of mitochondrial
338 Pi in this context, by inhibiting glycolysis using 2-deoxyglucose (2DG). WT, but not *mir1Δ*,
339 increased their OCR (respiration) upon a 1-hour treatment with 2DG (Figure 5B). Consistent
340 with this, mitotracker fluorescence increased with an increase in 2DG in WT, but not in *mir1Δ*
341 (Figure 5-figure supplement 1A). We further asked if the mitochondrial Pi transporter itself
342 glucose repressed, and therefore assessed Mir1 amounts in high and low glucose. Mir1 levels
343 are higher upon a shift to low glucose, and in cells grown in 2% ethanol, suggesting that Mir1
344 is glucose repressed (Figure 5C, Figure 5-figure supplement 1B). These data suggest that
345 mitochondrial Pi transport is necessary for increasing mitochondrial activity after glucose
346 derepression.

347 We next asked whether just adding external Pi was sufficient to increase
348 mitochondrial activity, when cells are in high glucose. In medium supplemented with excess
349 Pi, the internal Pi increases as seen earlier (Figure 3C). Therefore, a simplistic assumption
350 would be that the addition of external Pi to cells in high glucose would also increase
351 mitochondrial Pi. However, an alternate possibility presents itself whererin since glycolytic
352 flux is already high in glucose, supplementing Pi will continue to fuel glycolysis. Indeed, this
353 was originally obseved by Harden and Young in 1908, where adding Pi increased fermentation
354 (46). In such a scenario, mitochondrial Pi will not increase. We estimated mitochondrial Pi in
355 this condition where excess Pi was externally supplemented. Notably, cells grown in high Pi
356 had decreased mitochondrial Pi (Figure 5-figure supplement 1C), without any changes in total
357 mitochondria volume or amounts (Figure 5-figure supplement 1D). Furthermore, directly
358 adding Pi to cells growing in high glucose also decreased basal OCR (Figure 5-figure

359 supplement 1E), consistent with decreased mitochondrial Pi. These data indicate that in high
360 glucose, simply supplementing Pi will not increase Pi access to the mitochondria. We
361 therefore now asked, if we inhibit glycolytic flux and then supplement Pi, what would happen
362 to mitochondrial activity. For this, we treated cells with 2DG, and subsequently added Pi and
363 measured the OCR (Figure 5-figure supplement 1F). In this case, supplementing Pi increased
364 the basal OCR (Figure 5-figure supplement 1F). Collectively, these data suggest that a
365 combination of decreasing glycolysis and increasing Pi can together increase respiration.
366 Next, in order to directly test mitochondrial activation based on external Pi availability, we
367 isolated mitochondria, and estimated activity *in vitro* upon adding increasing Pi.
368 Mitochondrial activity increased with increased Pi, with maximum activity observed with 25
369 mM Pi supplemented (Figure 5D). In a complementary experiment, we overexpressed the
370 Mir1 transporter in wild-type cells, to increase Pi within mitochondria (Figure 5-figure
371 supplement 1G). Mir1-OE cells have higher Cox2 levels and basal OCR (Figure 5E, 5F).
372 Therefore, increasing Pi transport to mitochondria is sufficient to increase mitochondrial
373 activity in high glucose.

374 Mitochondrial pyruvate transport is also required for mitochondrial respiration (47).
375 We asked where Pi availability stands in a hierarchy of constraints for mitochondrial
376 derepression, as compared to mitochondrial pyruvate transport. We measured the amounts
377 of the Mpc3 subunit of the mitochondrial pyruvate carrier (MPC) complex (47, 48). Mpc3
378 protein increases in *ubp3Δ* (Figure 5-figure supplement 1H). This also correlated with the
379 unimpaired TCA cycle flux (Figure 2-figure supplement 2D) and the increased mitochondrial
380 activity. Interestingly, in *ubp3Δ* grown in low Pi, Mpc3 further increased (Figure 5-figure
381 supplement 1H), but as shown earlier this condition cannot increase OCR or mitochondrial
382 activity (Figure 4F, Figure 4-figure supplement 1F). Basal Mpc3 levels decrease in *mir1Δ*, but
383 upon shifting to 0.1% glucose, Mpc3 increases in both WT and *mir1Δ*, with higher levels in
384 *mir1Δ* (Figure 5-figure supplement 1I). Therefore, even where Mpc3 is high (*ubp3Δ* in low Pi,
385 and *mir1Δ* in low glucose), mitochondrial activity remains low if Pi is restricted (Figure 4F, 4H).
386 There was also no decrease in basal OCR in *mpc3Δ* in high glucose, and the basal OCR
387 increased to the same level as of WT after shifting to 0.1% glucose (Figure 5-figure supplement
388 1J). Since Mpc3 changes with mitochondrial Pi availability (Figure S5G, S5H), we also
389 measured Mpc3 in the Mir1OE. No further changes in Mpc3 were observed in Mir1OE (Figure

390 5-figure supplement 1K), indicating that increasing mitochondrial Pi alone need not increase
391 Mpc3. Overall, although Mpc3 levels corelate with decreased glycolysis (*ubp3Δ* - Figure 5-
392 figure supplement 1H, *ubp3Δ* in low Pi- Figure 5-figure supplement 1H, low glucose - Figure
393 5-figure supplement 1I), increased Mpc3 alone cannot increase mitochondrial activity and
394 respiration in the absence of adequate mitochondrial Pi.

395 Collectively, mitochondrial Pi availability constrains glucose-mediated mitochondrial
396 repression. Increasing available pools of Pi to enter the mitochondria is sufficient to induce
397 mitochondrial activity.

398 **Repression of mitochondrial respiration via Pi budgeting is conserved in Ubp3 mutants**
399 **across diverse yeast genetic backgrounds**

400 So far, we have identified a role for intracellular Pi budgeting as a constraint for
401 mitochondrial activity under high glucose. These were all carried out using a robust,
402 prototrophic yeast strain from a CEN.PK background. *S. cerevisiae* however, while Crabtree
403 positive, have tremendous genetic diversity (49). We therefore asked if this mitochondrial
404 repression through Pi budgeting (mediated by Ubp3 function) is conserved across other
405 strains of *S. cerevsiae* as well. To test this, we generated Ubp3 deletion mutants in different
406 genetic backgrounds of *S.* cerevsiae, including BY4742, W303 and Σ1278. In all these strain
407 backgrounds, we observed a significant increase in mitotracker fluorescne intensity and Cox2
408 protein levels in *ubp3Δ* (Figure 6A, B). This suggests the role of Ubp3 as a regulator of
409 mitochondrial repression, independent of the genetic background of the yeast (*S. cerevsiae*)
410 strain. To further assess if loss of Ubp3 shows a concurrent increase in Pi levels, we measured
411 the total Pi levels in WT and *ubp3Δ* in a W303 strain background. We observed a significant
412 increase in total Pi levels in *ubp3Δ* cells in this strain (Figure 6C), similar to what we observed
413 in the CEN.PK strain (Figure 3C). Finally, to test if the altered Pi budgeting regulates the
414 mitochondrial activity in these cells, we measured the basal OCR in WT, *ubp3Δ* and *ubp3Δ* in
415 low (1 mM) Pi medium, in the W303 strain background. Consistent with the increase in
416 mitotracker fluorescence intensity and Cox2 protein levels, we observed a significant increase
417 in the basal OCR in *ubp3Δ* cells (Figure 6D). This increase was not observed in *ubp3Δ* in a low
418 Pi medium (Figure 6D). This suggests that the role of altered Pi budgeting in regulating
419 mitochondrial respiration is conserved in other genetic backgrounds of *S. cerevisiae*.

420 Finally, we asked how important mitochondrial Pi transport was for growth, under
421 glycolytic inhibition. Consistent with the requirement for mitochondrial Pi transport to
422 increase mitochondrial respiration upon glycolytic inhibition (Figure 5B), WT cells only exhibit
423 a slightly decreased growth in the presence of 2DG (Figure 6E). In contrast, *mir1Δ* show a
424 severe growth defect upon 2DG treatment (Figure 6E), revealing a synergetic effect of
425 combining 2DG with inhibiting mitochondrial Pi transport. Therefore, the combined inhibition
426 of glycolysis and mitochondrial Pi transport restricts the growth of glycolytic cells.

427 Collectively, our data suggests a conserved role for intracellular Pi bugeting in
428 regulating mitochondrial repression in high glucose and the role of mitochondrial Pi transport
429 in regulating adaptation for growth under glycolytic inhibition.

430

431 **Discussion**

432 In this study, we highlight a role for Pi budgeting between cytosolic glycolysis and
433 mitochondrial processes (which compete for Pi) in constraining mitochondrial repression
434 (Figure 6F). Ubp3 controls this process (Figure 1), by maintaining the amounts of the glycolytic
435 enzymes Pfk1 and GAPDH (Tdh2 and Tdh3) and thereby allows high glycolytic flux. At high
436 fermentation rates, glycolytic enzymes levels at maximal activity maintain high glycolytic rates
437 (effectively following zero-order kinetics), and therefore, changes in the enzyme levels will
438 have a direct, proportionate effect on flux (50). The loss of Ubp3 decreases glycolytic flux,
439 resulting in a systems-level, mass-action based rewiring of glucose metabolism where more
440 G6P is routed towards trehalose synthesis and PPP (Figure 2, Figure 6F). Indeed, inhibiting just
441 phosphofructokinase can reroute glucose flux from glycolysis to PPP (51–53), and our study
442 now permits contextualized interpretations of these results. Such reallocations of glucose flux
443 will collectively increase overall Pi, coming from the combined effect of increased Pi release
444 from trehalose synthesis, and decreased Pi consumption via reduced GAPDH. This altered
445 intracellular Pi economy increases Pi pools available to mitochondria, and increasing
446 mitochondrial Pi is necessary and sufficient to increase respiration in high glucose (Figure 4,
447 Figure 5, Figure 6). Mitochondrial Pi transport maintains mitochondrial activity in high
448 glucose, and increases mitochondrial activity in low glucose (Figure 4, Figure 5). Finally, the

449 mitochondrial Pi transporter Mir1 itself decreases in high glucose (Figure 5). Therefore, this
450 glucose-dependent repression of Mir1 also restricts mitochondrial Pi availability (and thereby
451 activity) in high glucose.

452 Traditionally, loss-of-function mutants of metabolic enzymes are used to understand
453 metabolic state regulation. This approach negates nuanced investigations, since metabolic
454 enzymes are often essential for viability. Furthermore, metabolic pathways have multiple,
455 contextually regulated nodes, through which cells maintain their metabolic state. Therefore,
456 alternate approaches to identify global regulators of metabolic states (as opposed to single
457 enzymes), might uncover ways via which multiple nodes are simultaneously tuned, and can
458 reveal unanticipated systems-level principles of metabolic state rewiring. In this study of
459 glucose-mediated mitochondrial repression, the loss of the DUB Ubp3 decreases glycolytic
460 flux by reducing the enzymes at two critical nodes in the pathway - Pfk1 and GAPDH. Unlike
461 loss of function mutants, a reduction in amounts will only rewire metabolic flux. By 'hitting'
462 multiple steps in glycolysis simultaneously, *ubp3Δ* have decreased Pi consumption, as well as
463 increased Pi release. Such a cumulative phenomenon reveals more than inhibiting only
464 GAPDH, where increased Pi comes only from reduced Pi consumption, and not from increased
465 trehalose biosynthesis. Our serendipitous identification of a regulator which regulates
466 multiple steps in glucose metabolism to change the metabolic environment, now suggests a
467 general basis of mitochondrial regulation that would have otherwise remained hidden.
468 Separately, finding the substrates of Ubp3 and whether Ubp3 directly regulates glycolytic
469 enzymes are exciting future research questions requiring concurrent innovations in accessible
470 chemical-biological approaches to study DUBs.

471 Because phosphates are ubiquitous, it is challenging to identify hierarchies of Pi-
472 dependent processes in metabolic state regulation (35). Phosphate transfer reactions are the
473 foundation of metabolism, driving multiple, thermodynamically unfavorable reactions (54,
474 55). Contextually, the laws of mass action predict that the relative rates of these reactions will
475 regulate overall Pi balance, and contrarily the Pi allocation to Pi-dependent reactions will
476 determine reaction rates (35, 37). Additionally, cells might control Pi allocations for different
477 reactions via compartmentalizing Pi in organelles, to spatially restrict Pi availability (56–58).
478 Our data collectively suggest a paradigm where the combination of factors regulates
479 mitochondrial Pi and thereby activity. In glycolytic yeast cells growing in high glucose,

480 mitochondrial Pi availability becomes restricted due to higher utilization of Pi in glycolysis
481 compared to mitochondria. Consistent with this, a rapid decrease in Pi upon glucose addition
482 has been observed (18, 19, 39). Interesting, *in vitro* studies with isolated mitochondria from
483 tumor cells also find that decreasing Pi levels decreases respiration (19), which would be
484 consistent with this scenario. Further, supplementing Pi correlates with decreased
485 mitochondrial repression in tumors (18, 59). By increasing Pi through a systems-level rewiring
486 of glucose metabolism (such as in *ubp3Δ* cells), cells can collectively increase mitochondrial
487 access to Pi. This Pi budgeting determines mitochondrial activity. Supplementing Pi under
488 conditions of low glycolysis (where mitochondrial Pi transport is enhanced), as well as directly
489 supplementing Pi to isolated mitochondria, increases respiration (Figure 5, Figure 5-figure
490 supplement 1). Therefore, in order to derepress mitochondria, a combination of increased Pi
491 along with decreased glycolysis is required. An additional systems-level phenomenon that
492 might regulate Pi transport to the mitochondria is the decrease in cytosolic pH upon
493 decreased glycolysis (60, 61). The cytosolic pH in highly glycolytic cells is ~7, and decreasing
494 glycolysis results in cytosolic acidification (60, 61). Therefore, under conditions of decreased
495 glycolysis (2DG treatment, deletion of Ubp3, and decreased GAPDH activity), cytosolic pH
496 becomes acidic. Since mitochondrial Pi transport itself is dependent on the proton gradient,
497 a low cytosolic pH would favour mitochondrial Pi transport (62). Therefore, under conditions
498 of decreased glycolysis (2DG treatment, or loss of Ubp3, or decreased GAPDH activity), where
499 cytosolic pH would be acidic, increasing cytosolic Pi might indirectly increase mitochondria Pi
500 transport, thereby leading to increased respiration. Alternately, increasing mitochondrial Pi
501 transporter amounts can achieve the same result, as seen by overexpressing Mir1 (Figure 5).
502 A similar observation has been reported in *Arabidopsis*, reiterating an evolutionarily
503 conserved role for mitochondrial Pi in controlling respiration (63). Relatedly, glycolytic
504 inhibition can suppress cell proliferation in Warburg-positive tumors (64, 65), or inflammatory
505 responses (66). However, these cells survive by switching to mitochondrial respiration (67,
506 68), requiring alternate approaches to prevent their proliferation (69). Inhibiting
507 mitochondrial Pi transport in combination with glycolytic inhibition could restrict the
508 proliferation of Warburg/Crabtree positive cells.

509 Since its discovery in the 1920s, the phenomenon of accelerated glycolysis with
510 concurrent mitochondrial repression has been intensely researched. Yet, the biochemical

511 constraints for glucose-mediated mitochondrial repression remains unresolved. One
512 hypothesis suggests that the availability of glycolytic intermediates might determine the
513 extent of mitochondrial repression. F1,6BP inhibits complex III and IV of the electron transport
514 chain (ETC) in Crabtree positive yeast (14–17). Similarly, the ratio between G6P and F1,6BP
515 regulates the extent of mitochondrial repression (16, 17). Although G6P/F6P accumulates in
516 *ubp3Δ* (Figure 2C), this is not the case in *tdh2Δtdh3Δ* (GAPDH mutant) (Figure 3-figure
517 supplement 1D), suggesting that G6P/F6P accumulation in itself is not the criterion to increase
518 mitochondrial activity. Separately, the competition for common metabolites/co-factors
519 between glycolysis and respiration (such as ADP, Pi or pyruvate) could drive this phenomenon
520 (14, 18). Here we observe that Mpc3 mediated mitochondrial pyruvate transport alone
521 cannot increase respiration. An additional consideration is the possible contribution of
522 changes in ADP in regulating mitochondrial activity, where the use of ADP in glycolysis might
523 limit mitochondrial ADP. Therefore, when Pi changes as a consequence of glycolysis, it coud
524 be imagined that a change in ADP balance can coincidentally occur. However, prior studies
525 show that even though cytosolic ADP decreases in the presence of glucose, this does not limit
526 mitochondrial ADP uptake, or decrease respiration, due to the very high affinity of the
527 mitochondrial ADP transporter (14, 19). These collectively reiterate the importance of Pi
528 access and transport to mitochondria in constraining mitochondrial respiration. Indeed, this
529 interpretation can also contextually explain observations from other model systems where
530 mitochondrial Pi transport seems to regulate respiration (70, 71).

531 We parsimoniously suggest that Pi access to the mitochondria as a key constraint for
532 mitochondrial repression under high glucose. In a hypothetical scenario, a single-step event
533 in evolution, reducing mitochondrial Pi transporter amounts, and/or increasing glycolytic flux
534 (to deplete cytosolic Pi), will result in whole-scale metabolic rewiring to repress mitochondria.
535 More elaborate regulatory events can easily be imagined as subsequent adaptations to
536 enforce mitochondrial repression. Given the central role played by Pi, something as
537 fundamental as access to Pi will constrain mitochondrial repression. Concurrently, the rapid
538 incorporation of Pi into faster glycolysis can give cells a competitive advantage, while also
539 sequestering Pi in the form of usable ATP. Over the course of evolution, this could conceivably
540 drive other regulatory mechanisms to enforce mitochondrial repression, leading to the

541 currently observed complex regulatory networks and signaling programs observed in the
542 Crabtree effect, and other examples of glucose-dependent mitochondrial repression.

543

544 Materials and methods

545 Statistics and graphing

546 Unless otherwise indicated, statistical significance for all indicated experiments were
547 calculated using unpaired Student's t-tests (GraphPad prism 9.0.1). Graphs were plotted using
548 GraphPad prism 9.0.1

549 Yeast strains, media, and growth conditions

550 A prototrophic CEN.PK strain of *Saccharomyces cerevisiae* (WT) (72) was used unless
551 mentioned otherwise. Strains are listed in appendix table S1. Gene deletions, chromosomal
552 C-terminal tagged strains were generated by PCR mediated gene deletion/tagging (73).
553 Mitochondria targeted Mneon strain (Mito-mNeon green) is described in (31). The cox2-62
554 strain is described in (32). Media compositions, growth conditions and CRISPR-Cas9 based
555 mutagenesis are described in extended methods (SI appendix).

556 Mitotracker fluorescence

557 Mitotracker fluorescence was measured using Thermo Varioscan™ LUX multimode plate
558 reader (579/599 excitation/emission). Detailed protocol is described in extended methods.
559 Mitotracker fluorescence were normalized using OD_{600} of each sample and relative
560 fluorescence intensity calculated.

561 Protein extraction and Western blotting

562 Total protein was precipitated, extracted using trichloroacetic acid (TCA) as described earlier
563 (74). Blots were quantified using ImageJ software. Detailed protocol is described in extended
564 methods.

565 Basal OCR measurement

566 The basal OCR was measured using Agilent Seahorse XFe24 analyzer. Basal OCR readings were
567 normalized for cell number (using OD_{600} of samples) in each well. The detailed methods are
568 described in extended methods.

569 **Mitochondrial volume estimation**

570 High-resolution 3D fluorescence experiments were performed on an inverted confocal laser
571 scanning microscope (Carl Zeiss LSM 780 or Olympus FV3000). For each imaging field of view,
572 sequential z-stacks were acquired for each excitation channel. 488 nm laser excitation for
573 mNeonGreen and 561 nm laser excitation for Mitotracker CMXros dye were used
574 respectively. Images taken were deconvolved and analyzed further in ImageJ software with
575 custom-written routines. Mitochondria segmentation and quantification was done using the
576 Mitochondria Analyzer plugin (75) in Imagej. For visualization, maximum intensity projection
577 of 3D images was used.

578 **RNA extraction and RT-qPCR**

579 The RNA extraction was done using the hot phenol extraction method as described in (74).
580 The isolated RNA was DNase treated, and used for cDNA synthesis. Superscript III reverse
581 transcriptase enzyme (Invitrogen) was used for cDNA synthesis and RT-qPCR was performed
582 using KAPA SYBR FAST qRT PCR kit (KK4602, KAPA Biosystems). Taf10 was used as a control
583 for normalisation and the fold change in mRNA levels were calculated by 2^-ddct method.

584 **ATP, ethanol and Pi measurements**

585 ATP levels were measured by ATP estimation kit (Thermo Fisher A22066). Ethanol
586 concentration in the medium was estimated using potassium dichromate based assay
587 described in (76) with modifications. Pi was estimated using a malachite green phosphate
588 assay kit (Cayman chemicals, 10009325). Detailed sample collection and assay protocols are
589 described in extended methods.

590 **Metabolite extraction and analysis by LC-MS/MS**

591 The steady state levels and relative ^{13}C label incorporation into metabolites were estimated
592 by quantitative LC-MS/MS methods as described in (77). Detailed methodology is extensively
593 described in extended methods. Peak area measurements are listed in supplement file 1.

594 **Mitochondrial isolation**

595 Mitochondria was isolated by immunoprecipitation as described in (78, 79) with
596 modifications. The detailed protocol is described in extended methods (SI appendix). The
597 eluted mitochondria were used in malachite green assay for Pi estimation, boiled with SDS-
598 glycerol buffer for western blots or incubated with mitotracker CMXROS with mitochondria-
599 activation buffer for mitotracker assays.

600

601 **Data availability**

602 The LC-MS/MS peak area for all the metabolites can be found in supplement file 1. This study
603 includes no data deposited in external repositories.

604

605 **Acknowledgements**

606 We thank all SL lab members, Benjamin Tu, Anand Bachhawat and Vijay Jayaraman for
607 comments and suggestions. We acknowledge the NCBS/inStem/CCAMP mass spectrometry
608 facility for LC-MS/MS support. We thank Aayushee Khanna for help with experiments and
609 Gaurav Singh for help with microscopy. V.V acknowledges funding support from DST-INSPIRE
610 fellowship (IF170236) from the Department of Science and Technology (DST), Govt. of India,
611 S.N and SA acknowledges intramural funding from the DBT-inStem PhD program. S.L
612 acknowledges support from the DST SERB CRG grant CRG/2019/004772, a DBT-Wellcome
613 India Alliance Senior Fellowship (IA/S/21/2/505922), and institutional support from inStem.

614 **References**

615 1. J. Zhu, C. B. Thompson, Metabolic regulation of cell growth and proliferation. *Nat.*
616 *Rev. Mol. Cell Biol.* **20**, 436–450 (2019).

617 2. L. Cai, B. P. Tu, Driving the Cell Cycle Through Metabolism. *Annu. Rev. Cell Dev. Biol.*
618 **28**, 59–87 (2011).
619 3. D. L. (David L. Nelson, D. L. (David L. Nelson, A. L. Lehninger, M. M. Cox, Lehninger
620 principles of biochemistry (2008) (March 10, 2022).
621 4. O. Warburg, The metabolism of carcinoma cells 1. *J. Cancer Res.* **9**, 148–163 (1925).
622 5. M. G. Vander Heiden, L. C. Cantley, C. B. Thompson, Understanding the Warburg
623 Effect: The Metabolic Requirements of Cell Proliferation. *Science (80-.).* **324**, 1029–
624 1033 (2009).
625 6. H. G. Crabtree, Observations on the carbohydrate metabolism of tumours. *Biochem.*
626 *J.* **23**, 536–545 (1929).
627 7. R. H. De Deken, The Crabtree effect: a regulatory system in yeast. *J. Gen. Microbiol.*
628 **44**, 149–156 (1966).
629 8. L. Xia, *et al.*, The cancer metabolic reprogramming and immune response. *Mol.*
630 *Cancer* **20**, 1–21 (2021).
631 9. M. D. Kornberg, The immunologic Warburg effect: Evidence and therapeutic
632 opportunities in autoimmunity. *Wiley Interdiscip. Rev. Syst. Biol. Med.* **12**, 1–17
633 (2020).
634 10. N. Pacini, F. Borziani, Cancer stem cell theory and the warburg effect, two sides of the
635 same Coin? *Int. J. Mol. Sci.* **15**, 8893–8930 (2014).
636 11. A. M. Abdel-Haleem, *et al.*, The emerging facets of non-cancerous Warburg effect.
637 *Front. Endocrinol. (Lausanne).* **8**, 1–7 (2017).
638 12. E. Tsogtbaatar, C. Landin, K. Minter-Dykhouse, C. D. L. Folmes, Energy Metabolism
639 Regulates Stem Cell Pluripotency. *Front. Cell Dev. Biol.* **8**, 1–16 (2020).
640 13. A. Cornish-Bowden, Biochemical evolution : the pursuit of perfection. *Garl. Sci.*
641 (2016).
642 14. R. Diaz-Ruiz, M. Rigoulet, A. Devin, The Warburg and Crabtree effects: On the origin
643 of cancer cell energy metabolism and of yeast glucose repression. *Biochim. Biophys.*
644 *Acta - Bioenerg.* **1807**, 568–576 (2011).
645 15. N. Hammad, M. Rosas-Lemus, S. Uribe-Carvajal, M. Rigoulet, A. Devin, The Crabtree
646 and Warburg effects: Do metabolite-induced regulations participate in their
647 induction? *Biochim. Biophys. Acta - Bioenerg.* **1857**, 1139–1146 (2016).
648 16. R. Díaz-Ruiz, *et al.*, Mitochondrial Oxidative Phosphorylation Is Regulated by Fructose

649 1,6-Bisphosphate: A POSSIBLE ROLE IN CRABTREE EFFECT INDUCTION? *. *J. Biol.*
650 *Chem.* **283**, 26948–26955 (2008).
651 17. M. R. Lemus, *et al.*, The role of glycolysis-derived hexose phosphates in the induction
652 of the Crabtree effect. *J. Biol. Chem.* **293**, 12843–12854 (2018).
653 18. D. H. Koobs, Phosphate mediation of the Crabtree and Pasteur effects. *Science (80-.).*
654 **178**, 127–133 (1972).
655 19. S. Rodríguez-Enríquez, O. Juárez, J. S. Rodríguez-Zavala, R. Moreno-Sánchez, Multisite
656 control of the Crabtree effect in ascites hepatoma cells. *Eur. J. Biochem.* **268**, 2512–
657 2519 (2001).
658 20. F. Tripodi, R. Nicastro, V. Reghellin, P. Coccetti, Post-translational modifications on
659 yeast carbon metabolism: Regulatory mechanisms beyond transcriptional control.
660 *Biochim. Biophys. Acta - Gen. Subj.* **1850**, 620–627 (2015).
661 21. T. Hitosugi, J. Chen, Post-translational modifications and the Warburg effect.
662 *Oncogene* **33**, 4279–4285 (2014).
663 22. J. R. Broach, Nutritional control of growth and development in yeast. *Genetics* **192**,
664 73–105 (2012).
665 23. A. Hershko, A. Ciechanover, THE UBIQUITIN SYSTEM. *Annu. Rev. Biochem.* **67**, 425–79
666 (1998).
667 24. D. Komander, M. Rape, The Ubiquitin Code. *Annu. Rev. Biochem.* **81**, 203–229 (2012).
668 25. C. M. Pickart, M. J. Eddins, Ubiquitin: Structures, functions, mechanisms. *Biochim.*
669 *Biophys. Acta - Mol. Cell Res.* **1695**, 55–72 (2004).
670 26. E. Postma, C. Verduyn, W. A. Scheffers, J. P. Van Dijken, Enzymic analysis of the
671 crabtree effect in glucose-limited chemostat cultures of Saccharomyces cerevisiae.
672 *Appl. Environ. Microbiol.* **55**, 468–77 (1989).
673 27. B. Ossareh-Nazari, *et al.*, Cdc48 and Ufd3, new partners of the ubiquitin protease
674 Ubp3, are required for ribophagy. *EMBO Rep.* **11**, 548–554 (2010).
675 28. M. Isasa, *et al.*, Multiplexed, Proteome-Wide Protein Expression Profiling: Yeast
676 Deubiquitylating Enzyme Knockout Strains. *J. Proteome Res.* **14**, 5306–5317 (2015).
677 29. R. Nostramo, S. N. Varia, B. Zhang, M. M. Emerson, P. K. Herman, The Catalytic
678 Activity of the Ubp3 Deubiquitinating Protease Is Required for Efficient Stress Granule
679 Assembly in Saccharomyces cerevisiae. *Mol. Cell. Biol.* **36**, 173 (2016).
680 30. F. Fontanesi, I. C. Soto, D. Horn, A. Barrientos, Assembly of mitochondrial cytochrome

681 c-oxidase, a complicated and highly regulated cellular process. *Am. J. Physiol. - Cell*
682 *Physiol.* **291**, 1129–1147 (2006).
683 31. N. Dua, A. Seshadri, A. Badrinarayanan, DarT-mediated mtDNA damage induces
684 dynamic reorganization and selective segregation of mitochondria. *J. Cell Biol.* **221**
685 (2022).
686 32. N. Bonnefoy, N. Bsat, T. D. Fox, Mitochondrial Translation of Saccharomyces
687 cerevisiae COX2 mRNA Is Controlled by the Nucleotide Sequence Specifying the Pre-
688 Cox2p Leader Peptide. *Mol. Cell. Biol.* **21**, 2359–2372 (2001).
689 33. A. A. Shestov, *et al.*, Quantitative determinants of aerobic glycolysis identify flux
690 through the enzyme GAPDH as a limiting step. *Elife* **3**, 1–18 (2014).
691 34. R. Gupta, *et al.*, A tRNA modification balances carbon and nitrogen metabolism by
692 regulating phosphate homeostasis. *Elife* **8**, 1–33 (2019).
693 35. R. Gupta, S. Laxman, Cycles, sources, and sinks: Conceptualizing how phosphate
694 balance modulates carbon flux using yeast metabolic networks. *Elife* **10**, 1–14 (2021).
695 36. P. W. Mason, D. P. Carbone, R. A. Cushman, A. S. Waggoner, The importance of
696 inorganic phosphate in regulation of energy metabolism of Streptococcus lactis. *J.*
697 *Biol. Chem.* **256**, 1861–1866 (1981).
698 37. J. H. Van Heerden, *et al.*, Lost in transition: Start-up of glycolysis yields subpopulations
699 of nongrowing cells. *Science (80-.).* **343** (2014).
700 38. P. C. Brazy, L. J. Mandel, V. W. Dennis, S. R. Gullans, Metabolic Requirement for
701 Inorganic Phosphate by the Rabbit Proximal Tubule: EVIDENCE FOR A CRABTREE
702 EFFECT Metabolic Requirement for Inorganic Phosphate by the Rabbit Proximal
703 Tubule EVIDENCE FOR A CRABTREE EFFECT. *J Clin Invest* **70**, 53 (1982).
704 39. S. Hohmann, W. Bell, M. J. Neves, D. Valckx, J. M. Thevelein, Evidence for trehalose-6-
705 phosphate-dependent and-independent mechanisms in the control of sugar influx
706 into yeast glycolysis. *Mol. Microbiol.* **20**, 981–991 (1996).
707 40. T. Hunter, Why nature chose phosphate to modify proteins. *Philos. Trans. R. Soc. B*
708 *Biol. Sci.* **367**, 2513–2516 (2012).
709 41. P. O. Ljungdahl, B. Daignan-Fornier, Regulation of amino acid, nucleotide, and
710 phosphate metabolism in Saccharomyces cerevisiae. *Genetics* **190**, 885–929 (2012).
711 42. S. Austin, A. Mayer, Phosphate Homeostasis − A Vital Metabolic Equilibrium
712 Maintained Through the INPHORS Signaling Pathway. *Front. Microbiol.* **11**, 1367

713 (2020).
714 43. J. M. Mouillon, B. L. Persson, New aspects on phosphate sensing and signalling in
715 Saccharomyces cerevisiae. *FEMS Yeast Res.* **6**, 171–176 (2006).
716 44. H. Murakami, G. Blobel, D. Pain, Isolation and characterization of the gene for a yeast
717 mitochondrial import receptor. *Nat. 1990 3476292* **347**, 488–491 (1990).
718 45. V. Zara, *et al.*, Yeast mitochondria lacking the phosphate carrier/p32 are blocked in
719 phosphate transport but can import preproteins after regeneration of a membrane
720 potential. *Mol. Cell. Biol.* **16**, 6524–6531 (1996).
721 46. A. Harden, W. J. Young, The alcoholic Ferment of Yeast-juice.Part III.-The Function of
722 Phosphates in the Fermentation o f Glucose hy Yeast-juice. *Proc. R. Soc. London. Ser.*
723 *B,* **80**, 299–311 (1908).
724 47. A. Timoń-Gómez, M. Proft, A. Pascual-Ahuir, Differential Regulation of Mitochondrial
725 Pyruvate Carrier Genes Modulates Respiratory Capacity and Stress Tolerance in Yeast.
726 *PLoS One* **8**, e79405 (2013).
727 48. T. Bender, G. Pena, J.-C. Martinou, Regulation of mitochondrial pyruvate uptake by
728 alternative pyruvate carrier complexes. *EMBO J.* **34**, 911–924 (2015).
729 49. J. Peter, *et al.*, Genome evolution across 1,011 Saccharomyces cerevisiae isolates.
730 *Nature* **556**, 339–344 (2018).
731 50. P. Grigaitis, B. Teusink, An excess of glycolytic enzymes under glucose-limited
732 conditions may enable Saccharomyces cerevisiae to adapt to nutrient availability.
733 *FEBS Lett.* (2022) https:/doi.org/10.1002/1873-3468.14484 (November 28, 2022).
734 51. W. Yi, *et al.*, PFK1 Glycosylation Is a Key Regulator of Cancer Cell Growth and Central
735 Metabolic Pathways. *Science* **337**, 975 (2012).
736 52. H. Miyazawa, *et al.*, Rewiring of embryonic glucose metabolism via suppression of
737 PFK-1 and aldolase during mouse chorioallantoic branching. *Dev.* **144**, 63–73 (2017).
738 53. W. D. Hollinshead, *et al.*, Examining Escherichia coli glycolytic pathways, catabolite
739 repression, and metabolite channeling using Δpfk mutants. *Biotechnol. Biofuels* **9**, 1–
740 13 (2016).
741 54. F. H. Westheimer, Why Nature Chose Phosphates. *Science (80-.).* **235**, 1173–1178
742 (1987).
743 55. S. C. L. Kamerlin, P. K. Sharma, R. B. Prasad, A. Warshel, Why nature really chose
744 phosphate. *Q. Rev. Biophys.* **46**, 1–132 (2013).

745 56. J. W. Booth, G. Guidotti, Phosphate Transport in Yeast Vacuoles *. *J. Biol. Chem.* **272**,
746 20408–20413 (1997).
747 57. T. Vila, S. Frases, F. M. Gomesid, Lessons from protozoans: Phosphate sensing and
748 polyphosphate storage in fungi. *PLOS Pathog.* **18**, e1010298 (2022).
749 58. M. E. Solesio, *et al.*, Depletion of mitochondrial inorganic polyphosphate (polyP) in
750 mammalian cells causes metabolic shift from oxidative phosphorylation to glycolysis.
751 *Biochem. J.* **478**, 1631–1646 (2021).
752 59. M. Brin, R. W. McKee, The Inhibition of Respiration by Glucose, Fructose, and
753 Mannose in the Ehrlich Mouse Ascites Tumor. *Cancer Res.* **16**, 364–368 (1956).
754 60. R. Orij, S. Brul, G. J. Smits, Intracellular pH is a tightly controlled signal in yeast.
755 *Biochim. Biophys. Acta - Gen. Subj.* **1810**, 933–944 (2011).
756 61. R. Dechant, *et al.*, Cytosolic pH is a second messenger for glucose and regulates the
757 PKA pathway through V-ATPase. *EMBO J.* **29**, 2515–2526 (2010).
758 62. P. Hamel, *et al.*, Redundancy in the function of mitochondrial phosphate transport in
759 Saccharomyces cerevisiae and Arabidopsis thaliana. *Mol. Microbiol.* **51**, 307–317
760 (2004).
761 63. F. Jia, *et al.*, Overexpression of Mitochondrial Phosphate Transporter 3 Severely
762 Hampers Plant Development through Regulating Mitochondrial Function in
763 Arabidopsis. *PLoS One* **10**, e0129717 (2015).
764 64. H. Pelicano, D. S. Martin, R. Xu, P. Huang, Glycolysis inhibition for anticancer
765 treatment. 4633–4646 (2006).
766 65. S. O'Neill, R. K. Porter, N. McNamee, V. G. Martinez, L. O'Driscoll, 2-Deoxy-D-Glucose
767 inhibits aggressive triple-negative breast cancer cells by targeting glycolysis and the
768 cancer stem cell phenotype. *Sci. Rep.* **9**, 1–11 (2019).
769 66. G. Soto-Heredero, M. M. Gómez de las Heras, E. Gabandé-Rodríguez, J. Oller, M.
770 Mittelbrunn, Glycolysis – a key player in the inflammatory response. *FEBS J.* **287**,
771 3350–3369 (2020).
772 67. R. Shiratori, *et al.*, Glycolytic suppression dramatically changes the intracellular
773 metabolic profile of multiple cancer cell lines in a mitochondrial metabolism-
774 dependent manner. *Sci. Rep.* **9**, 1–15 (2019).
775 68. C. L. Lu, *et al.*, Tumor Cells Switch to Mitochondrial Oxidative Phosphorylation under
776 Radiation via mTOR-Mediated Hexokinase II Inhibition - A Warburg-Reversing Effect.

PLoS One **10**, e0121046 (2015).

69. G. Cheng, *et al.*, Mitochondria-targeted drugs synergize with 2-deoxyglucose to trigger breast cancer cell death. *Cancer Res.* **72**, 2634–2644 (2012).

70. M. Scheibye-Knudsen, B. Quistorff, Regulation of mitochondrial respiration by inorganic phosphate; comparing permeabilized muscle fibers and isolated mitochondria prepared from type-1 and type-2 rat skeletal muscle. *Eur. J. Appl. Physiol.* **105**, 279–287 (2009).

71. E. L. Seifert, E. Ligeti, J. A. Mayr, N. Sondheimer, G. Hajnóczky, The mitochondrial phosphate carrier: Role in oxidative metabolism, calcium handling and mitochondrial disease. *Biochem. Biophys. Res. Commun.* **464**, 369–375 (2015).

72. J. B. J.P. van Dijken, *et al.*, An interlaboratory comparison of physiological and genetic properties of four Saccharomyces cerevisiae strains. *Enzyme Microb. Technol.* **26**, 706–714 (2000).

73. M. S. Longtine, *et al.*, Additional modules for versatile and economical PCR-based gene deletion and modification in Saccharomyces cerevisiae. *Yeast* **14**, 953–961 (1998).

74. V. Vengayil, Z. Rashida, S. Laxman, The E3 ubiquitin ligase Pib1 regulates effective gluconeogenic shutdown upon glucose availability. *J. Biol. Chem.* **294**, 17209–17223 (2019).

75. A. Chaudhry, R. Shi, X. D. S. Luciani, INNOVATIVE METHODOLOGY A pipeline for multidimensional confocal analysis of mitochondrial morphology , function , and dynamics in pancreatic □ -cells. *Am. J. Physiol. - Endocrinol. Metab.* **318**, 87–101 (2019).

76. M. Sriariyanun, P. Mutrakulcharoen, S. Tepaamorndech, K. Cheenkachorn, K. Rattanaporn, A Rapid Spectrophotometric Method for Quantitative Determination of Ethanol in Fermentation Products. *Orient. J. Chem.* **35**, 744–750 (2019).

77. A. Walvekar, Z. Rashida, H. Maddali, S. Laxman, A versatile LC-MS / MS approach for comprehensive , quantitative analysis of central metabolic pathways [version 1 ; peer review : 2 approved]. 1–15 (2018).

78. P. C. Liao, I. R. Boldogh, S. E. Siegmund, Z. Freyberg, L. A. Pon, Isolation of mitochondria from Saccharomyces cerevisiae using magnetic bead affinity purification. *PLoS One* **13**, 1–15 (2018).

809 79. W. W. Chen, E. Freinkman, D. M. Sabatini, Rapid immunopurification of mitochondria
810 for metabolite profiling and absolute quantification of matrix metabolites. *Nat.*
811 *Protoc.* **12**, 2215 (2017).
812
813

814 **Figure legends**

815 **Figure 1: A deubiquitinase deletion screen identifies Ubp3 as a regulator of glucose-**
816 **mediated mitochondrial repression**

817 A) Schematic depicting glucose-mediated mitochondrial repression (Crabtree effect).

818 B) Schematic describing the screen with a yeast DUB KO library to identify regulators of
819 Crabtree effect.

820 C) Identifying DUB knockouts with altered mitochondrial potential. Heat map shows relative
821 mitochondrial membrane potential of 19 deubiquitinase deletions in high glucose, from 2
822 biological replicates. Also see figure 1-figure supplements 1A, B.

823 D) The deubiquitinase activity of Ubp3 and repression of mitochondrial membrane potential.
824 WT, *ubp3Δ,* and Ubp3^{C469A} were grown in high glucose and relative mitochondrial membrane
825 potential was measured. Data represent mean ± SD from three biological replicates (n=3).
826 Also see figure 1-figure supplement 1 D.

827 E) Effect of loss of Ubp3 on ETC complex IV subunit Cox2. WT and *ubp3Δ* were grown in high
828 glucose, and Cox2 was measured (western blot using an anti-Cox2 antibody). A representative
829 blot (out of 3 biological replicates, n=3) and their quantifications are shown. Data represent
830 mean ± SD.

831 F) Basal oxygen consumption rate (OCR) in high glucose in *ubp3Δ*. WT and *ubp3Δ* were grown
832 in high glucose, and OCR was measured. Basal OCR corresponding to ~3 x 10^5 cells, from two
833 independent experiments (n=2), normalized to the OD_{600} is shown. Bar graph representations
834 are shown in the inset. Data represent mean ± SD.

835 G) Total ATP levels in *ubp3Δ* and WT. WT and *ubp3Δ* were grown in high glucose, and total
836 ATP were measured. Data represent mean ± SD from three biological replicates (n=3).

837 H) Dependence of *ubp3Δ* on mitochondrial ATP. WT and *ubp3Δ* cells were grown in high
838 glucose, and treated with 1 mM sodium azide for 45 minutes. Total ATP levels in sodium azide
839 treated and untreated cells were measured. Data represent mean ± SD (n=3).

840 I) Requirement for mitochondrial respiration in high glucose in *ubp3Δ*. A growth curve of WT
841 and *ubp3Δ* in high glucose in the presence of OXPHOS uncoupler FCCP (10 µM), and serial
842 dilution growth assay in high glucose in the presence/absence of sodium azide (1 mM) are
843 shown. Data represent mean ± SD (n=2). Also see figure 1-figure supplement 1 H, I.

844 Data information: **p<0.01, ***p<0.001.

845

846 **Figure 2: Key glycolytic enzymes decrease and glucose flux is rerouted in *ubp3Δ* cells**

847 A) A schematic illustrating directions of glucose-6-phosphate (G6) flux in cells. Glucose is
848 converted to G6P, a precursor for trehalose, the pentose phosphate pathway (PPP), and
849 glycolysis.

850 B) Effect of loss of Ubp3 on key glycolytic enzymes. WT and *ubp3Δ* were grown in high glucose
851 and the Pfk1, Tdh2, and Tdh3 levels were measured by western blot using an anti-FLAG
852 antibody. A representative blot (out of three biological replicates, n=3) and their
853 quantification are shown. Data represent mean ± SD. Also see figure 2-figure supplement 1A.

854 C) Steady-state metabolite amounts in WT and *ubp3Δ* in high glucose. Relative steady-state
855 levels of trehalose, major glycolytic, and PPP intermediates were estimated in WT and *ubp3Δ*.
856 Data represent mean ± SD from three biological replicates (n=3). Also see Appendix Table S3.

857 D) Relative glycolytic and trehalose synthesis flux in WT and *ubp3Δ*. Relative ^{13}C-label
858 incorporation into trehalose and glycolytic intermediates, after a pulse of 1% $^{13}C_6$ glucose is
859 shown. Data represent mean ± SD from three biological replicates (n=3). Also see Appendix
860 Table S3, figure 2-figure supplement 1 D, E.

861 E) Ethanol production in *ubp3Δ*. WT and *ubp3Δ* were grown in high glucose and ethanol in the
862 media was measured. Data represent mean ± SD from three biological replicates (n=3).

863 F) Relative rate of ethanol production in WT vs *ubp3Δ*. WT and *ubp3Δ* were grown in high
864 glucose (to OD_{600} ~ 0.6), equal numbers of cells were shifted to fresh medium (high glucose)
865 and ethanol concentration in the medium was measured temporally. Data represent mean ±
866 SD from three biological replicates (n=3)

867 Data information: *p<0.05, **p<0.01, ***p<0.001.

868

869 **Figure 3: Rerouted glucose flux results in phosphate (Pi) accumulation**

870 A) Changes in protein levels in *ubp3Δ* (dataset from Isasa et al., 2015). *ubp3Δ* cells have an
871 increase in proteins involved in mitochondrial respiration and decrease in proteins involved
872 in glucose and phosphate metabolism.

873 B) Schematic showing maintenance of Pi balance during glycolysis. Trehalose synthesis from
874 G6P releases Pi, and the conversion of G3P to 1,3BPG by GAPDH consumes Pi. In *ubp3Δ*,
875 trehalose biosynthesis (which releases Pi) increases. *ubp3Δ* have decreased GAPDH, which
876 will decrease Pi consumption. This increase in Pi release along with decreased Pi consumption
877 could increase cytosolic Pi.

878 C) Intracellular Pi levels in WT and *ubp3Δ*. WT and *ubp3Δ* were grown in high glucose and the
879 total free phosphate (Pi) levels were estimated. WT in high Pi (2% glucose, 10mM Pi) was a
880 positive control. Data represent mean ± SD from three biological replicates (n=3). Also see
881 figure 3-figure supplement 1A.

882 D) Pho regulon responses in WT and *ubp3Δ*. Protein levels of Pho84-FLAG and Pho12-FLAG
883 were compared between WT grown in high glucose and in high Pi, *ubp3Δ* in high glucose with
884 or without a shift to a no-Pi medium for one hour, by western blot. A representative blot (out
885 of three biological replicates, n=3) and their quantifications are shown. Data represent mean
886 ± SD.

887 E) Contribution of trehalose synthesis as a Pi source. WT, *tps2Δ*, *ubp3Δ,* and *ubp3Δtps2Δ* were
888 grown in high glucose and the total Pi levels were estimated. Data represent mean ± SD from
889 three biological replicates (n=3). Also see figure 3-figure supplement 1B.

890 F) Loss of GAPDH isozymes Tdh2 and Tdh3 and effect on Pi. WT, *ubp3Δ,* and *tdh2Δtdh3Δ* were
891 grown in high glucose and total Pi was estimated. Data represent mean ± SD from three
892 biological replicates (n=3).

893 G) Pi levels in *ubp3Δ* and *tdh2Δtdh3Δ* cells in ethanol medium. WT, *ubp3Δ,* and *tdh2Δtdh3Δ*
894 cells were grown in ethanol medium and the total Pi levels were estimated. Data represent
895 mean ± SD from three biological replicates (n=3).

896 Data information: *p<0.05, **p<0.01, ***p<0.001, ****p<0.0001.

897

898 **Figure 4: Mitochondrial Pi availability correlates with mitochondrial activity in *ubp3Δ***

899 A) A hypothetical mechanism of cytosolic free Pi controling mitochondrial activity by
900 regulating mitochondrial Pi availability.

901 B) Mitochondrial Pi amounts in WT vs *ubp3Δ*. Mitochondria were isolated by
902 immunoprecipitation from WT and *ubp3Δ* and mitochondrial Pi estimated. Mitochondrial Pi
903 levels (normalised to Idh1) are shown. Data represent mean ± SD from three biological
904 replicates (n=3). Also see figure 4-figure supplement 1A, B.

905 C) Cox2 protein in *tdh2Δtdh3Δ*. WT, *ubp3Δ,* and *tdh2Δtdh3Δ* were grown in high glucose and
906 Cox2 protein was estimated. A representative blot (out of three biological replicates, n=3) and
907 their quantifications are shown. Data represent mean ± SD.

908 D) Basal OCR levels in *tdh2Δtdh3Δ*. WT, *ubp3Δ,* and *tdh2Δtdh3Δ* were grown in high glucose
909 and basal OCR was measured from two independent experiments (n=2). Data represent mean
910 ± SD. Also see figure 4-figure supplement 1C.

911 E) Comparative Pi amounts and Cox2 levels in *ubp3Δ*, *tdh2Δtdh3Δ,* WT cells. WT cells were
912 grown in high glucose, *ubp3Δ* and *tdh2Δtdh3Δ* were grown in high glucose and low Pi, and
913 Cox2 protein was estimated. A representative blot (out of three biological replicates, n=3) and
914 their quantifications are shown. Data represent mean ± SD. Also see figure figure 4-figure
915 supplement 1D, F.

916 F) Pi amounts and basal OCR in *ubp3Δ* and *tdh2Δtdh3Δ* vs WT cells. WT cells were grown in
917 high glucose, *ubp3Δ* and *tdh2Δtdh3Δ* were grown in high glucose and low Pi, and basal OCR
918 was measured from three independent experiments (n=3). Data represent mean ± SD.

919 G) Effect of loss of mitochondrial Pi transporter Mir1 on Cox2protein. WT, *ubp3Δ*, *mir1Δ,* and
920 *mir1Δubp3Δ* were grown in high glucose and Cox2 amounts compared. A representative blot
921 (out of three biological replicates, n=3) and their quantifications are shown. Data represent
922 mean ± SD.

923 H) Relationship of mitochondrial Pi transport and basal OCR in WT vs *ubp3Δ*. WT, *ubp3Δ*,
924 *mir1Δ,* and *mir1Δubp3Δ* cells were grown in high glucose and basal OCR was measured from
925 two independent experiments (n=2). Data represent mean ± SD.

926 Data information: *p<0.05, **p<0.01, ****p<0.0001.

927

928 **Figure 5: Mitochondrial Pi availability constrains mitochondrial activity under high glucose**

929 A) Relationship of mitochondrial Pi transport and respiration after glucose removal. WT and
930 *mir1Δ* cells were cultured in high (2%) glucose and shifted to low (0.1%) glucose for 1 hour.
931 The normalized basal OCR, from two independent experiments (n=2) are shown. Data
932 represent mean ± SD.

933 B) Requirement of mitochondrial Pi transport for switch to respiration upon glycolytic
934 inhibition by 2DG. WT and *mir1Δ* cells were cultured in high glucose and treated with or
935 without 0.25% 2DG for 1 hour. Basal OCR was measured from two independent experiments
936 (n=2). Data represent mean ± SD. Also see figure 5-figure supplement 1A.

937 C) Glucose-dependent regulation of Mir1. Cells (with Mir1-HA) were grown in high glucose
938 and shifted to low glucose (0.1% glucose) for 1 hour, and Mir1 levels compared. A
939 representative blot (out of three biological replicates, n=3) and their quantifications are
940 shown. Data represent mean ± SD. Also see figure 5-figure supplement 1B.

941 D) Increasing Pi concentrations and mitochondrial activity in isolated mitochondria.
942 Mitochondria were isolated from WT cells grown in high glucose, incubated with 1 mM
943 pyruvate, 1 mM malate, 0.5 mM ADP and 0-50 mM KH_2PO_4. The mitochondrial activity was
944 estimated by mitotracker fluorescence intensity, and intensities relative to the sample with 0
945 mM KH_2PO_4 is shown. Data represent mean ± SD from three biological replicates (n=3).

946 E) Effect of overexpressing Mir1 on Cox2 protein. WT (containing empty vector) and Mir1
947 overexpressing (Mir1OE) cells were grown in high glucose and Cox2 levels were estimated. A
948 representative blot (out of three biological replicates, n=3) and their quantifications are
949 shown. Data represent mean ± SD. Also see figure S5F.

950 F) Effect of overexpressing Mir1 on basal OCR. The basal OCR in WT (containing empty vector)
951 and Mir1OE in high glucose was measured from three independent experiments (n=3). Data
952 represent mean ± SD.

953 Data information: *p<0.05, **p<0.01, ***p<0.001.

954

955 **Figure 6: Repression of mitochondrial respiration via Pi budgeting is conserved in Ubp3**
956 **mutants across diverse yeast genetic backgrounds**

957 A) Effect of loss of Ubp3 on mitochondrial membrane potential in different yeast strains. WT
958 and *ubp3Δ* cells (in CEN.PK, BY4742, W303 and Σ1278 strains of *S. cerevisiae*) were grown in
959 high glucose and relative mitochondrial membrane potential was measured. Data represent
960 mean ± SD from three biological replicates (n=3).

961 B) Effect of loss of Ubp3 on ETC complex IV subunit Cox2. WT and *ubp3Δ* (in BY4742, W303
962 and Σ1278 strains of *S. cerevisiae*) were grown in high glucose, and Cox2 was measured. A
963 representative blot (out of 3 biological replicates, n=3) and their quantifications are shown.
964 Data represent mean ± SD.

965 C) Intracellular Pi levels in WT and *ubp3Δ* in W303 strain background. WT and *ubp3Δ* (in W303
966 strain background) were grown in high glucose and the total free phosphate (Pi) levels were
967 estimated. Data represent mean ± SD from three biological replicates (n=3).

968 D) Effect of low Pi on the basal OCR in WT and *ubp3Δ* cells in W303 strain background. WT
969 cells were grown in high glucose and *ubp3Δ* were grown in high glucose and low Pi, and basal
970 OCR was measured. Data represent mean ± SD (n=3).

971 E) Requirement of mitochondrial Pi transport for growth after 2DG treatment. Shown are
972 serial dilution growth assays in high glucose in the presence and absence of 0.1% 2DG, using
973 WT and *mir1Δ* cells. The results after 40hrs incubation/30°C are shown.

974 F) A model illustrating how mitochondrial Pi availability controls mitochondrial activity. In high
975 glucose, the decreased Pi due to high Pi consumption in glycolysis, along with the glucose-
976 mediated repression of mitochondrial Pi transporters, decreases mitochondrial Pi availability.
977 This reduces mitochondrial activity. In low glucose, increased mitochondrial Pi transporters
978 and lower glycolytic flux increases mitochondrial Pi, leading to enhanced mitochondrial
979 activity. In *ubp3Δ* cells in high glucose, high trehalose synthesis and lower glycolytic flux
980 results in an increase in Pi. This increases mitochondrial Pi availability and thereby the
981 mitochondrial activity.

982 Data information: *$p<0.05$, **$p<0.01$, ***$p<0.001$.

983

984

985

986

987

988

989

990

991

992

993

994 ## Supplement figure legends

995 **Figure 1-figure supplement 1: DUB screen details and further characterization of Ubp3**
996 **functions**

997 A) A list of the known/identified *S. cerevisiae* deubiquitinase enzymes is shown. The DUBs
998 which were used in this study, and the mitotracker intensity of two biological replicates (n=2)
999 relative to WT are shown.

1000 B) WT cells grown in a respiratory, ethanol medium and mitotracker fluorescence intensity
1001 compared to glucose medium. WT cells were grown in high glucose medium (2% glucose) and
1002 ethanol medium (2% ethanol), and the mitochondrial membrane potential was measured.
1003 Data from two independent experiments (n=2) is shown. Data represent mean ± SD.

1004 C) Representative images of WT and *ubp3Δ* cells treated with mitotracker red CMXROS.

1005 D) Schematic representation of the conserved domains of Ubp3 and its mammalian ortholog
1006 Usp10. The catalytic cysteine of Usp10 and Ubp3 is highlighted.

1007 E) The catalytically inactive mutant of Ubp3, Ubp3^{C469A} does not have altered Ubp3 protein
1008 levels. WT and Ubp3^{C469A} cells containing endogenous Ubp3 tagged with 3xFLAG (C terminus)
1009 were grown in high glucose and the protein levels of Ubp3 were measured. A representative
1010 blot (out of three biological replicates, n=3) and their quantification are shown. Data
1011 represent mean ± SD.

1012 F) The total mitochondrial volume does not change in *ubp3Δ* cells. WT and *ubp3Δ* cells with
1013 mitochondria targeted mNeon green were imaged, and the total mitochondrial volume per
1014 cell (n=104 for WT, n=107 for *ubp3Δ*) was calculated. A representative image and
1015 quantification are shown. Data represent mean ± SD.

1016 G) Tom70 protein amounts do not change in *ubp3Δ* cells. WT and *ubp3Δ* cells containing
1017 endogenous Tom70 tagged at the C terminus with a 3xFLAG epitope were grown in high
1018 glucose and the protein levels of Tom70 were measured by western blot. A representative
1019 blot (out of three biological replicates, n=3) and their quantification are shown. Data
1020 represent mean ± SD.

1021 H) Dependence of *ubp3Δ* on mitochondrial respiration. WT and *ubp3Δ* cells were grown in
1022 high glucose with or without mitochondrial inhibitor oligomycin (25 µM), and the OD_{600} was
1023 measured at different time points. Data represent mean ± SD (n=2).

1024 I) Dependence of *ubp3Δ* on functional mitochondrial respiration. Ubp3 deletions were done
1025 in respiration defective strains -Rho0, cox2-62, *atp1Δ* and *atp10Δ*, and serial dilution growth
1026 assay was done in high glucose. The results after 24 hours of incubation at 30°C are shown.

1027

1028 **Figure 2-figure supplement 1: Further estimates of glycolytic enzymes and flux**

1029 A) Loss of Ubp3 does not change the protein levels of enolase isozymes Eno1 and Eno2. WT
1030 and *ubp3Δ* cells containing Eno1 and Eno2 C terminus endogenously tagged with a 3x FLAG
1031 epitope, were grown in high glucose and protein amounts were estimated. A representative
1032 blot (out of three biological replicates, n=3) is shown in the lower panel, quantifications
1033 shown in the upper panel. Data represent mean ± SD.

1034 B) The decreased levels of glycolytic enzymes in *ubp3Δ* cells is not because of proteasomal
1035 degradation. WT and *ubp3Δ* were grown in high glucose and *ubp3Δ* cells were treated with
1036 or without MG132 (100 µM) for 30 minutes. Pfk1, Tdh2, and Tdh3 levels were measured by
1037 western blot using an anti-FLAG antibody. A representative blot (out of three biological
1038 replicates, n=3) and their quantification are shown. Data represent mean ± SD.

1039 C) Loss of Ubp3 results in decreased transcription of PFK1, TDH2 and TDH3 genes. WT, *ubp3Δ*
1040 and $Ubp3^{C469A}$ cells were grown in high glucose and the mRNA levels of PFK1, TDH2 and TDH3
1041 were analysed by RT-qPCR. The fold changes in mRNA levels are shown. Data represent mean
1042 ± SD.

1043 D) Steady-state pyruvate levels in WT and *ubp3Δ* in high glucose. Data represent mean ± SD
1044 from three biological replicates (n=3). Also see Appendix Table S3.

1045 E) Schematic showing the experimental design for measuring ^{13}C label incorporation into
1046 glycolytic intermediates and trehalose using a $^{13}C_6$ glucose-pulse.

1047 F) Changes in ^{13}C label incorporation into glycolytic intermediates and trehalose with time,
1048 and linearity of label incorporation after a pulse of 1% $^{13}C_6$ glucose is shown.

1049

1050 **Figure 2- figure supplement 2: Estimation of steady state levels and flux of TCA cycle**
1051 **intermediates**

1052 A) Steady-state TCA metabolite amounts in WT and *ubp3Δ* in high glucose. Relative steady-
1053 state levels of TCA cycle intermediates were estimated in WT and *ubp3Δ*. Data represent
1054 mean ± SD from three biological replicates (n=3). Also see Appendix Table S3.

1055 B) Schematic showing the experimental design for measuring ^{13}C label incorporation into TCA
1056 cycle intermediates using a $^{13}C_6$ glucose-pulse.

1057 C) Changes in ^{13}C label incorporation into TCA cycle intermediates with time, and linearity of
1058 label incorporation after a pulse of 1% $^{13}C_6$ glucose is shown.

1059 D) Relative TCA cycle flux in WT and *ubp3Δ*. Relative ^{13}C-label incorporation into TCA cycle
1060 intermediates, after a pulse of 1% $^{13}C_6$ glucose is shown. Data represent mean ± SD from three
1061 biological replicates (n=3). Also see Appendix Table S3.

1062 Data information: *p<0.05

1063

1064 **Figure 3-figure supplement 1: Comparisons of phosphate, ethanol and other metabolites in**
1065 **WT, *ubp3Δ* and GAPDH mutants**

1066 A) Loss of Ubp3 deubiquitinase activity and Pi levels. WT, *ubp3Δ,* and $Ubp3^{C469A}$ cells were
1067 grown in high glucose and the total free phosphate (Pi) levels were estimated. Data from two
1068 independent experiments (n=2) is shown. Data represent mean ± SD. B) Trehalose levels in
1069 WT and *ubp3Δ* cells in the absence of Tps2. *tps2Δ* and *ubp3Δtps2Δ* cells were grown in high
1070 glucose, and the trehalose levels were estimated using targeted LC-MS/MS. Data represent
1071 mean ± SD from three biological replicates (n=3).

1072 C) Loss of GAPDH isozymes Tdh2 and Tdh3 and ethanol production. WT and *tdh2Δtdh3Δ* cells
1073 were grown in high glucose and the ethanol concentration in the medium was measured.
1074 Data are represented as mean ± SD from three biological replicates (n=3). Note: The WT
1075 shown here is same as the WT in Figure 2E, the ethanol assays in Figure 2E and Figure S3C
1076 were done together and a common WT control was used.

1077 D) Steady state levels of glycolytic intermediates: *tdh2Δtdh3Δ* cells have unaltered steady
1078 state levels of G6P/F6P, increased levels of F1,6 BP and G3P and decreased levels of 3PG and
1079 PEP. WT and *tdh2Δtdh3Δ* cells were grown in high glucose and the steady state amounts of
1080 glycolytic intermediates were estimated using targeted LC-MS/MS. Data represent mean ± SD
1081 from three biological replicates (n=3). Also see Appendix Table S3.

1082 E) Trehalose levels in *tdh2Δtdh3Δ* cells. WT and *tdh2Δtdh3Δ* cells were grown in high glucose
1083 and trehalose amounts were estimated using targeted LC-MS/MS. Data represent mean ± SD
1084 from three biological replicates (n=3).

1085 Data information: *p<0.05, **p<0.01.

1086

1087 **Figure 4-figure supplement 1: Mitochondrial Pi estimation characterizations and**
1088 **correlations of mitochondrial activity with Pi availability**

1089 A) Lack of vacuolar contamination in mitochondria isolated by immunoprecipitation.
1090 Mitochondria were isolated from WT cells grown in high glucose and the protein levels of
1091 Tom20, Cox2, Idh1 and Vph1 and were measured in cell lysate and immunoprecipitated
1092 mitochondria by western blot.

1093 B) Idh1 levels in *ubp3Δ* cells and WT cells grown in high Pi. WT cells were grown in high
1094 glucose, or high glucose and high Pi medium (10mM Pi) and *ubp3Δ* cells were grown in high
1095 glucose, and the Idh1 protein levels were estimated by western blot. A representative blot
1096 (out of three biological replicates, n=3) is shown in the lower panel. Quantification is shown
1097 in the upper panel. Data represent mean ± SD.

1098 C) Mitochondrial membrane potential in *tdh2Δtdh3Δ* cells. WT, *ubp3Δ,* and *tdh2Δtdh3Δ* cells
1099 were grown in high glucose and the mitochondrial membrane potential was measured. Data
1100 represent mean ± SD from three biological replicates (n=3).

1101 D) Pi levels in *ubp3Δ* cells grown in low Pi (1mM Pi) vs WT cells. WT cells were grown in high
1102 glucose and *ubp3Δ* cells were grown in high glucose or high glucose-low Pi, and the total Pi
1103 levels were estimated. Data represent mean ± SD from three biological replicates (n=3).

1104 E) Ethanol production in *ubp3Δ* cells grown in a low Pi medium. WT cells were grown in high
1105 glucose and *ubp3Δ* cells were grown in high glucose or high glucose-low Pi, and the ethanol
1106 concentration in the medium was measured. Data represent mean ± SD from three biological
1107 replicates (n=3).

1108 F) Pi amounts and mitochondrial membrane potential in WT, *ubp3Δ,* and *tdh2Δtdh3Δ* cells.
1109 The cells were grown in high glucose or high glucose-low Pi, and the mitochondrial membrane
1110 potential was measured. Data from two independent experiments (n=2) is shown. Data
1111 represent mean ± SD.

1112 G) The Pi mediated change in basal OCR in *ubp3Δ* is dependent on mitochondrial respiration.
1113 WT and Rho0 cells were grown in high glucose, Rho0/*ubp3Δ* were grown in high glucose and
1114 low Pi, and basal OCR was measured from three independent experiments (n=3). Data
1115 represent mean ± SD.

1116 H) The protein levels of mitochondrial Pi transporters Mir1 and Pic2 in *ubp3Δ* cells. WT and
1117 *ubp3Δ* cells containing endogenously tagged Mir1 and Pic2 at their C terminus with a 6x HA
1118 epitope tag were grown in high glucose and Mir1 and Pic2 proteins were measured by
1119 western blot. A representative blot (out of three biological replicates, n=3) is shown in the
1120 lower panel. Quantification is shown in the upper panel. Data represent mean ± SD.

1121 Data information: *p<0.05, **p<0.01, ***p<0.001.

1122

1123 **Figure 5-figure supplement 1: Mitochondrial phosphate and pyruvate transport**
1124 **relationships with mitochondrial activity**

1125 A) Requirement of Mir1 for switching to increased mitochondrial activity upon 2-
1126 deoxyglucose (2-DG) treatment. WT and *mir1Δ* cells were grown in high glucose and treated
1127 with 0.1% and 0.25% 2-DG for one hour. The mitochondrial membrane potential was
1128 measured from two independent experiments (n=2). Data represent mean ± SD.

1129 B) Mir1 protein levels and glucose repression. Cells containing Mir1 endogenously tagged at
1130 the C terminus with a 6x HA epitope tag were grown in high glucose or a respiratory medium
1131 (2% ethanol). Mir1 protein was estimated by western blot. A representative blot (out of three
1132 biological replicates, n=3) is shown in the lower panel. Quantification is shown in the upper
1133 panel. Data represent mean ± SD.

1134 C) Effect of supplementing Pi in the medium on mitochondrial Pi. WT cells were grown in high
1135 glucose, and high glucose, high Pi medium (10 mM Pi), mitochondria was isolated and the
1136 mitochondrial Pi levels were estimated. The mitochondrial Pi levels normalised to Idh1
1137 protein levels is shown. Data represent mean ± SD from three biological replicates (n=3). Also
1138 see supplementary figure S4B.

1139 D) Effect of supplementing Pi on the total mitochondrial volume. WT cells with mitochondria
1140 targeted mNeon green were grown in high glucose, and high glucose, high Pi medium (10 mM
1141 Pi), cells were imaged and the total mitochondrial volume per cell was calculated.

1142 E) Increasing Pi concentration in a high glucose medium results in a decrease in basal OCR.
1143 WT cells were grown in high glucose medium (YPD-Pi medium), supplemented with 5 mM Pi
1144 and at OD_{600}~0.6, the medium was supplemented with Pi (10 mM and 25 mM final
1145 concentrations). The basal OCR was measured one hour after Pi supplementation. Data
1146 represent mean ± SD from three biological replicates (n=3).

1147 E) Effect of increasing the Pi concentration in a high glucose medium, in the presence of 2DG,
1148 on basal OCR. WT cells were grown in high glucose medium (YPD-Pi medium), supplemented
1149 with 5 mM Pi and at OD_{600}~0.6, the medium was supplemented with Pi (25 mM final
1150 concentration) and 2DG (0.25%) for one hour and the basal OCR was measured. Data
1151 represent mean ± SD from three biological replicates (n=3).

1152 F) Overexpression of Mir1. C terminal 6x HA epitope-tagged Mir1 was expressed under G6PD
1153 promoter in cells with Mir1 endogenously tagged at the C terminus with a 6x-HA epitope tag.
1154 WT cells (carrying an empty vector, and expressing Mir1-HA under the endogenous Mir1
1155 promoter) and Mir1-OE cells were grown in high glucose. The protein levels of Mir1 were
1156 estimated by western blot, and clones with an ~2-fold increase in Mir1 were selected. A
1157 representative blot (out of three biological replicates, n=3) is shown in the lower panel.
1158 Quantification is shown in the upper panel. Data represent mean ± SD.

1159 G) Mpc3 protein levels in *ubp3Δ* cells. WT and *ubp3Δ* cells containing endogenously tagged
1160 Mpc3 at the C terminus with a 3x FLAG epitope tag, were cultured in high glucose (2% glucose)
1161 and high glucose-low Pi (2% glucose, 1 mM Pi). The Mpc3 protein levels were measured by
1162 western blot. A representative blot (out of three biological replicates, n=3) is shown in the
1163 lower panel, quantifications shown in the upper panel. Data represent mean ± SD.

1164 H) Mpc3 protein amounts upon shifting WT and *mir1Δ* cells to a low-glucose medium. WT and
1165 *mir1Δ* cells containing Mpc3-FLAG, were cultured in high glucose (2% glucose) and shifted to
1166 low (0.1%) glucose for 1 hour. Mpc3 protein was measured by western blot. A representative
1167 blot (out of three biological replicates, n=3) is shown in the lower panel, quantifications
1168 shown in the upper panel. Data represent mean ± SD.

1169 I) Requirement of Mpc3 for the increase in basal OCR upon shifting to low glucose. WT and
1170 *mpc3Δ* cells were cultured in high glucose (2% glucose) and shifted to low (0.1%) glucose for
1171 1 hour. The basal OCR from two independent experiments (n=2), normalized to the OD_{600} is
1172 shown. Data represent mean ± SD.

1173 J) Mpc3 levels and Mir1 overexpression. WT cells and Mir1-OE cells containing endogenously
1174 tagged Mpc3 ate the C terminus with a 3x FLAG tag were grown in high glucose. The protein
1175 levels of Mpc3 were estimated by western blot. A representative blot (out of three biological
1176 replicates, n=3) is shown in the panel. Quantification is shown in the upper panel. Data
1177 represent mean ± SD. Data information: *p<0.05, **p<0.01, ***p<0.001.

Figure 1: A deubiquitinase deletion screen identifies Ubp3 as a regulator of glucose-mediated mitochondrial repression

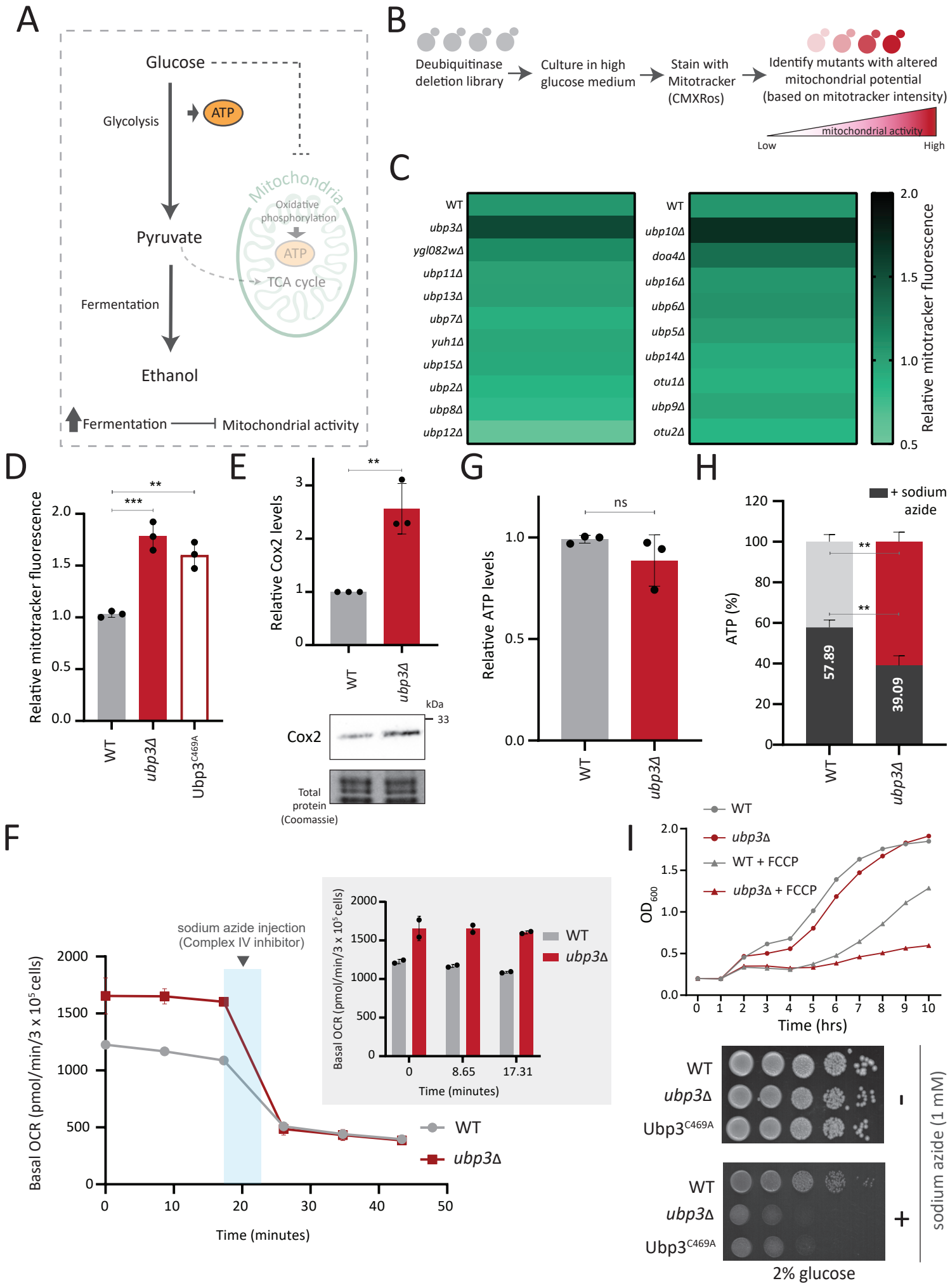

Figure 2: Key glycolytic enzymes decrease and glucose flux is rerouted in *ubp3Δ* cells

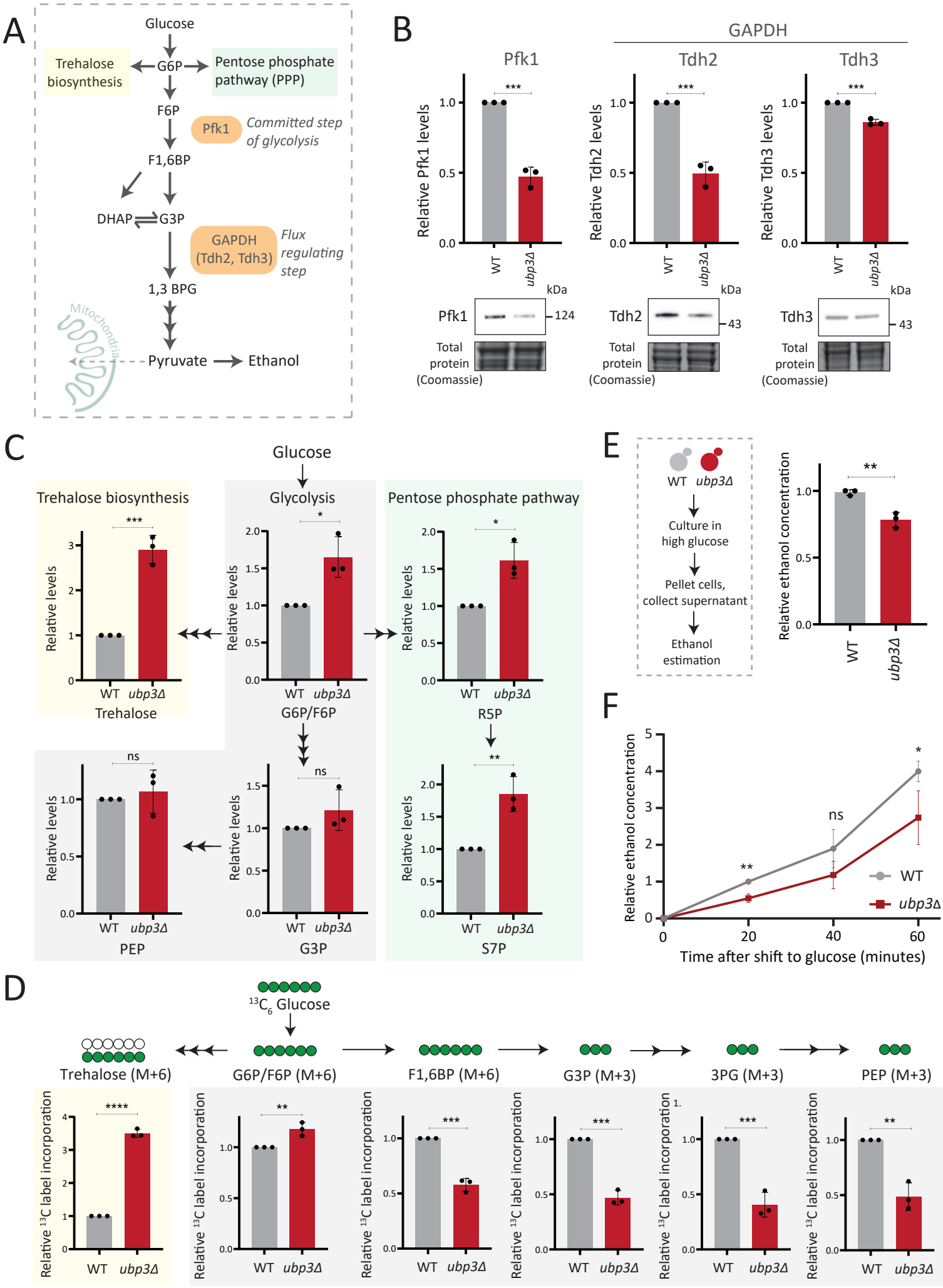

Figure 3: Rerouted glucose flux results in phosphate (Pi) accumulation

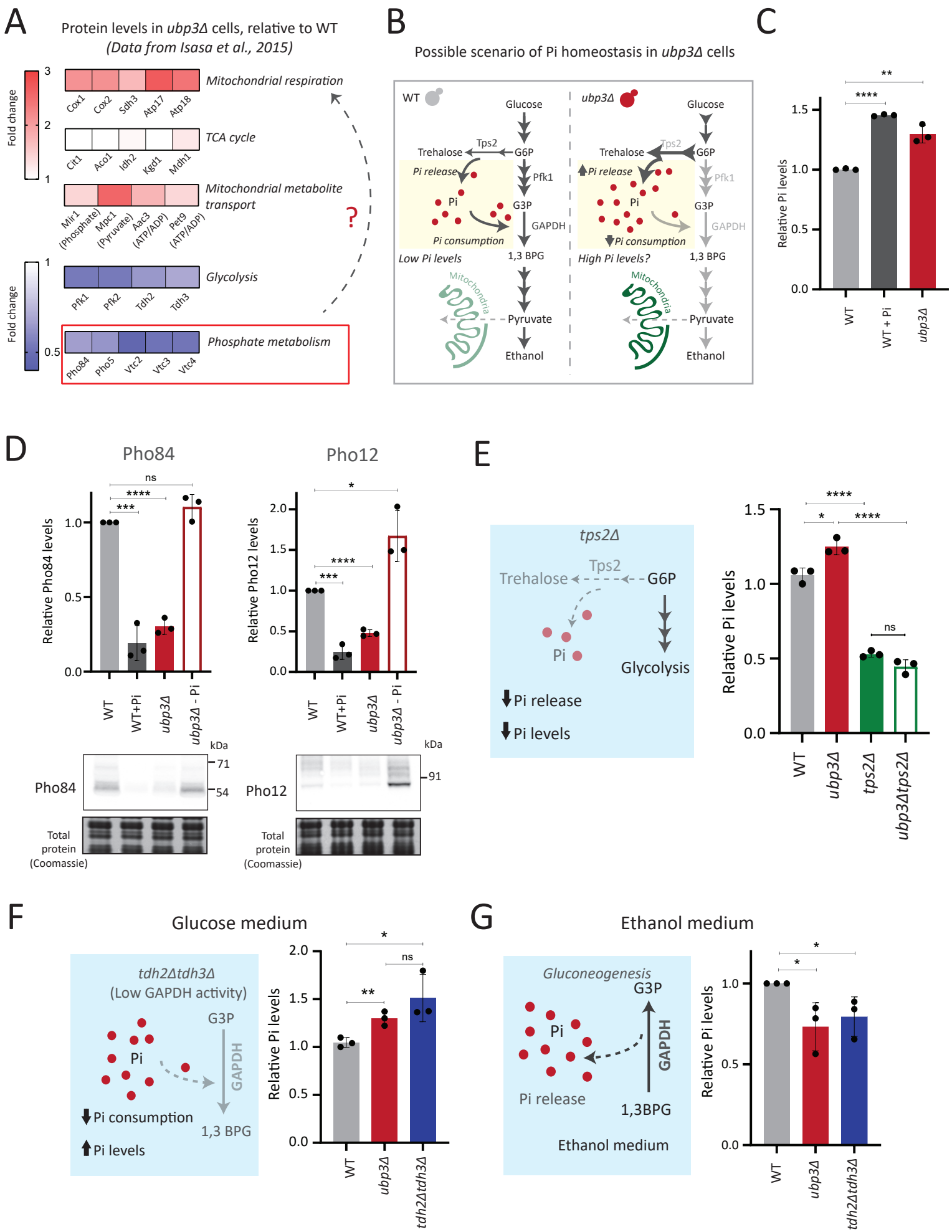

Figure 4: Mitochondrial Pi availability correlates with mitochondrial activity in *ubp3Δ*

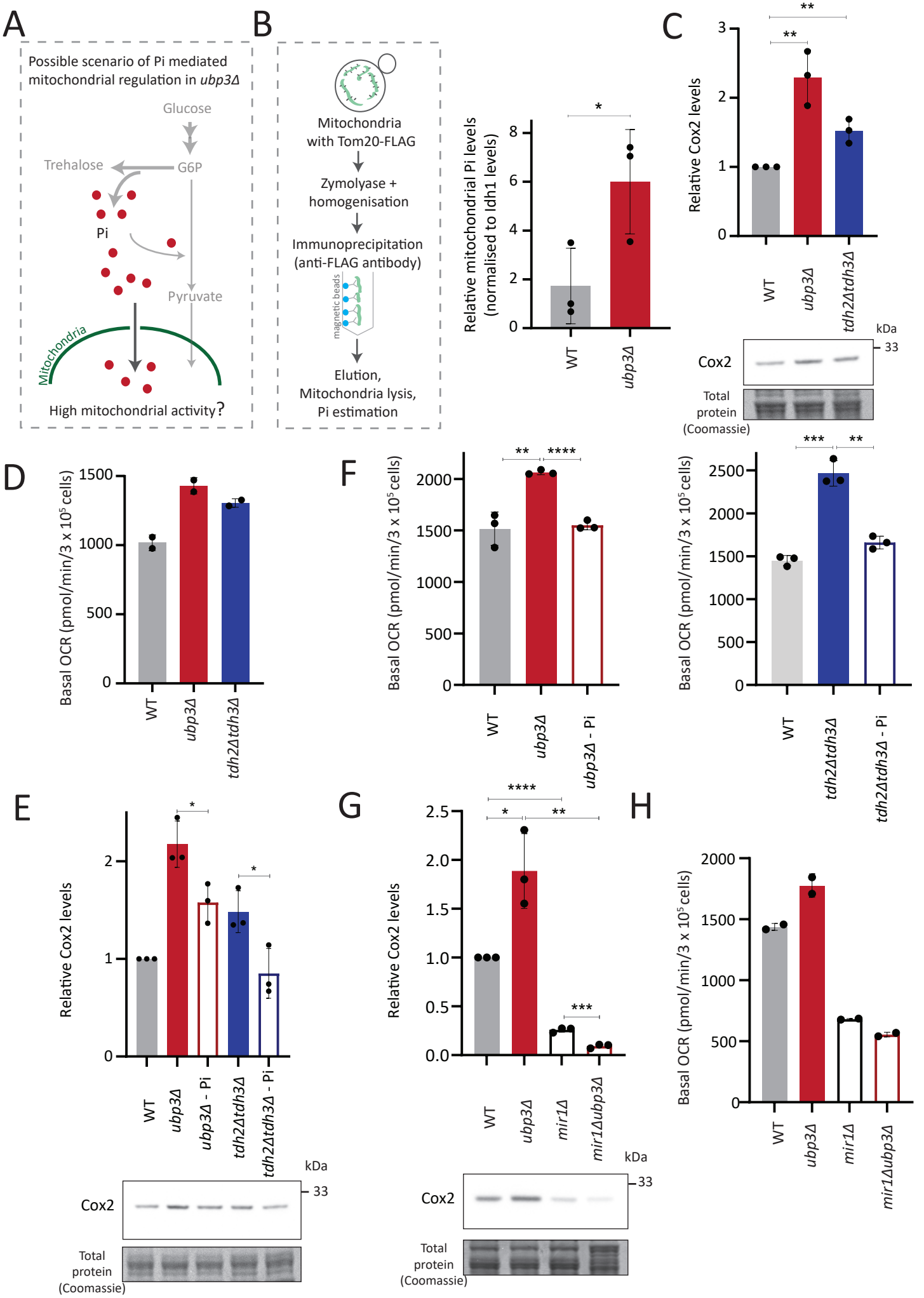

Figure 5: Mitochondrial Pi availability constrains mitochondrial activity under high glucose

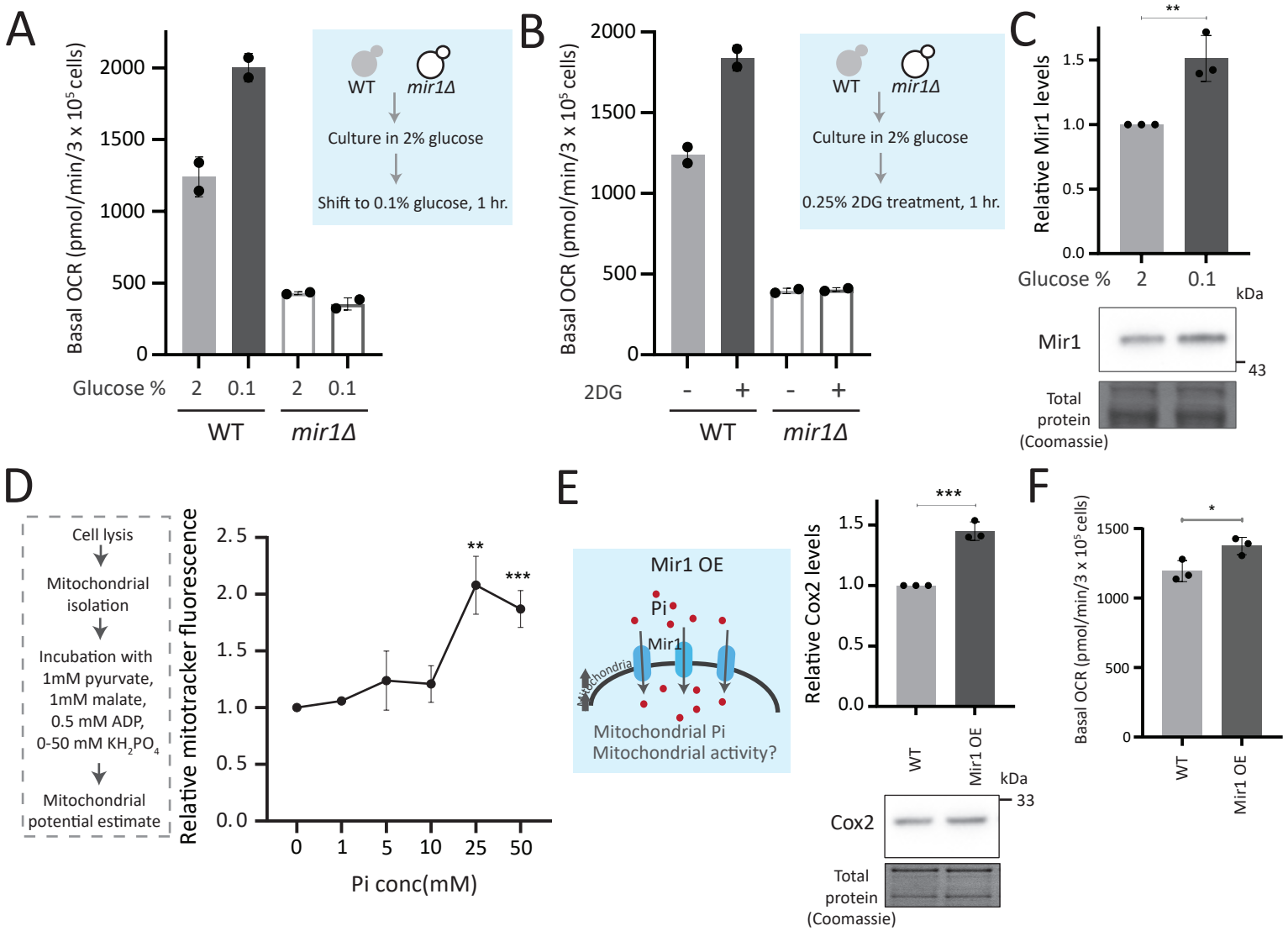

Figure 6: Repression of mitochondrial respiration via Pi budgeting is conserved in Ubp3 mutants across diverse yeast genetic backgrounds

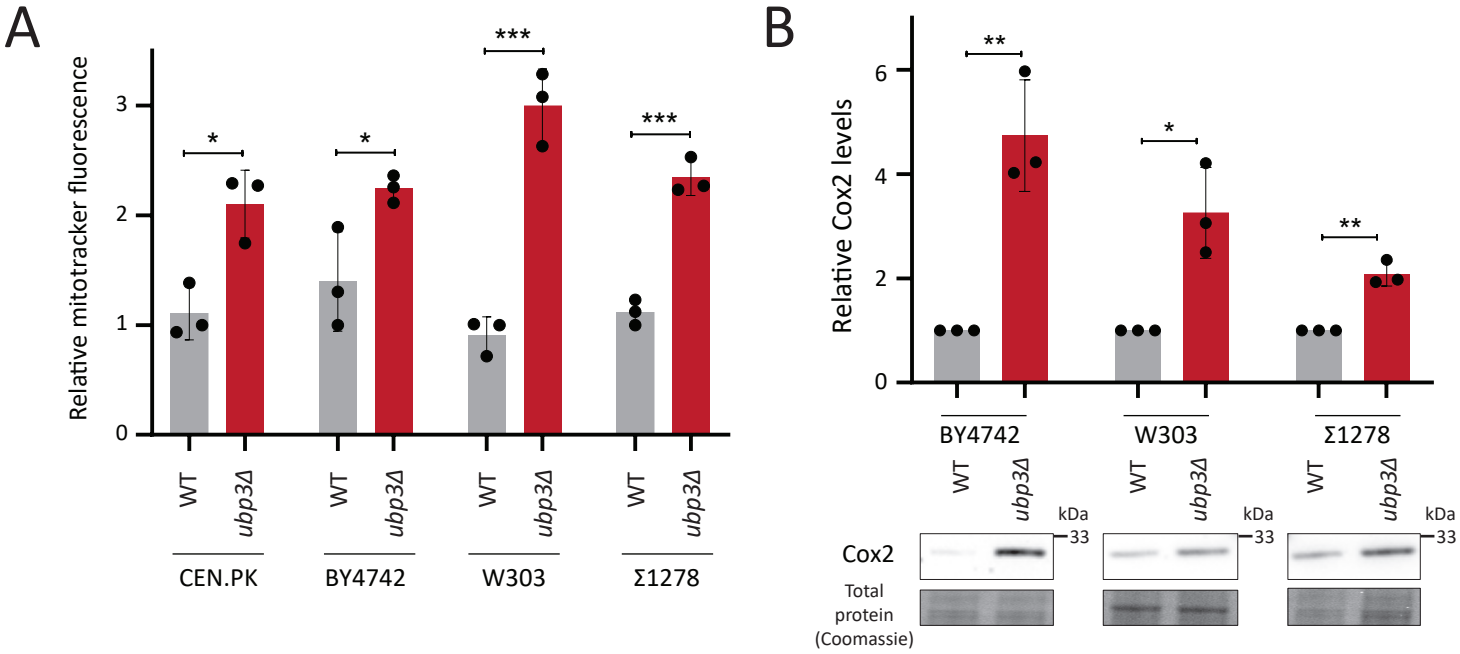

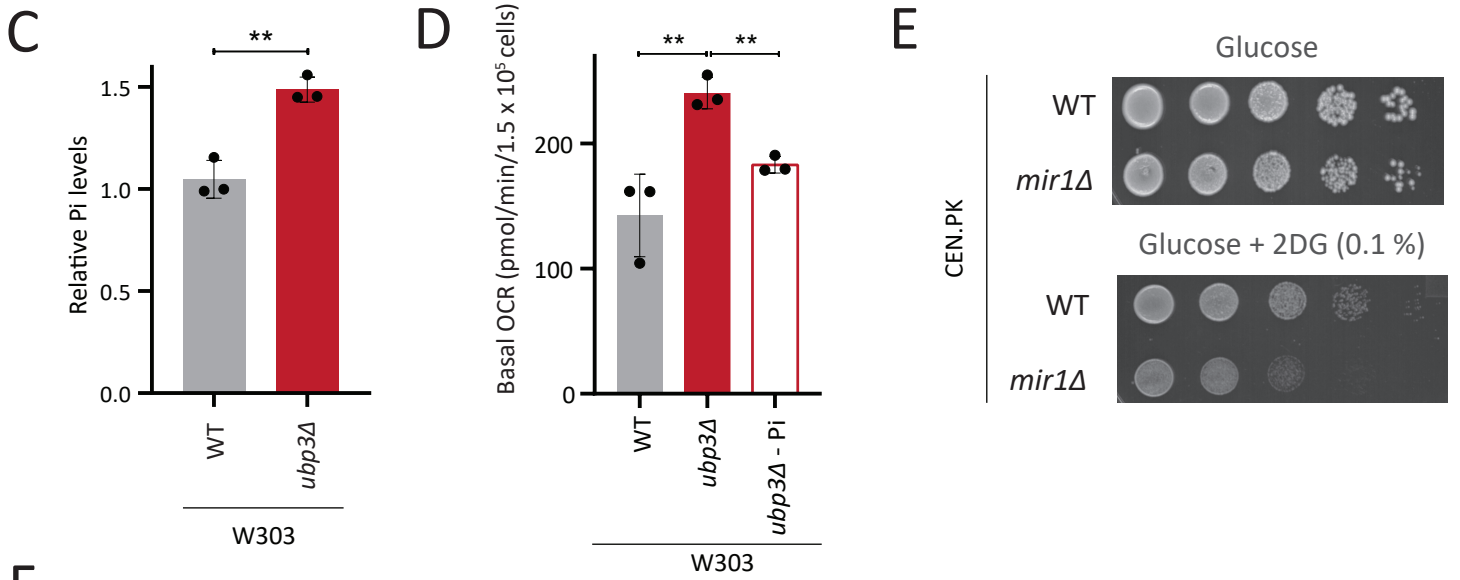

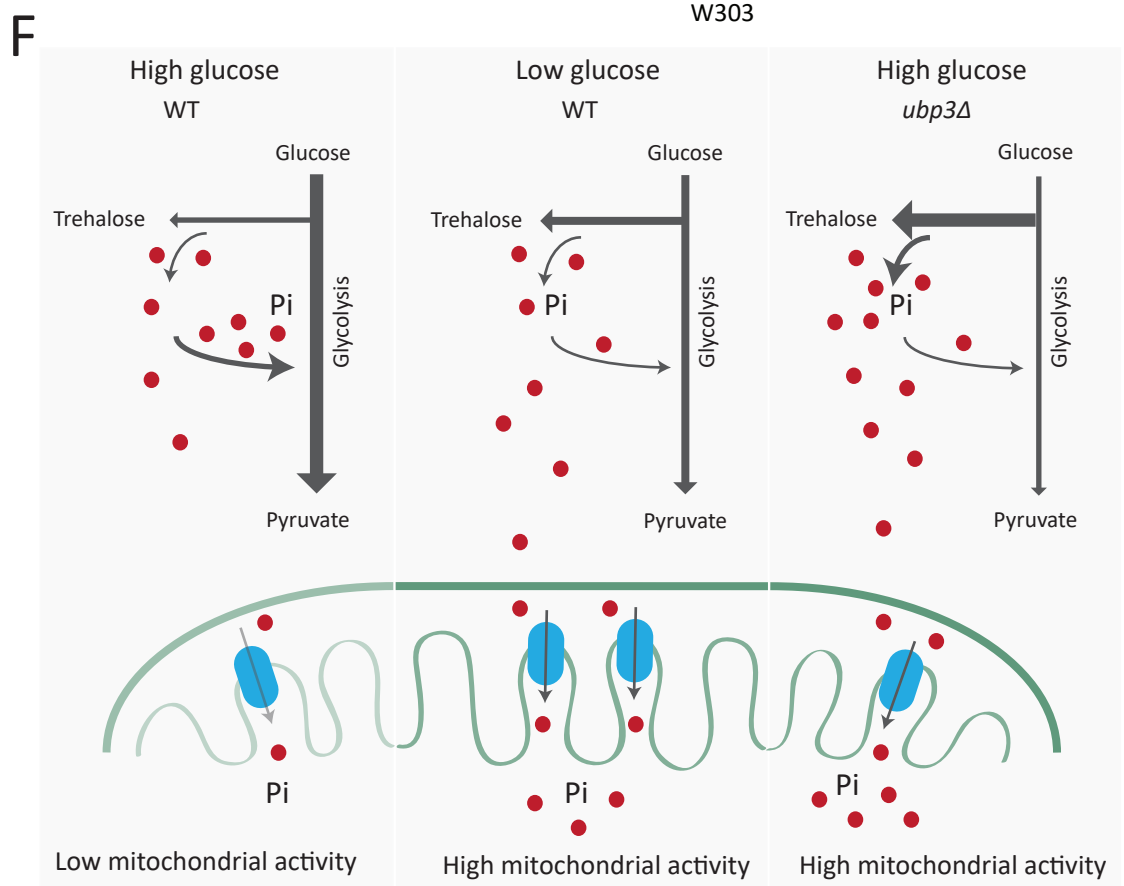

Figure 1-figure supplement 1: DUB screen details and further characterization of Ubp3 functions

A

Sl. No.	Gene name	Essential/non-essential	Deleted in this study (Yes/No)	Mitotracker intensity of the deletion mutant (Relative to WT)	
1	Ubp1	Non-essential	No. KOs were inviable	N/A	
2	Ubp2	Non-essential	Yes	0.832963	0.904247
3	Ubp3	Non-essential	Yes	1.446586	1.632793
4	Doa4	Non-essential	Yes	1.388516	1.221461
5	Ubp5	Non-essential	Yes	1.073892	0.987076
6	Ubp6	Non-essential	Yes	1.139659	1.040391
7	Ubp7	Non-essential	Yes	0.961557	0.847109
8	Ubp8	Non-essential	Yes	0.620714	0.98006
9	Ubp9	Non-essential	Yes	0.923033	1.000494
10	Ubp10	Non-essential	Yes	1.733428	1.636301
11	Ubp11	Non-essential	Yes	1.03262	0.961782
12	Ubp12	Non-essential	Yes	0.529191	0.602179
13	Ubp13	Non-essential	Yes	0.972874	1.027698
14	Ubp14	Non-essential	Yes	1.009835	0.864286
15	Ubp15	Non-essential	Yes	0.898673	0.97787
16	Ubp16	Non-essential	Yes	1.143826	0.993367
17	Yuh1	Non-essential	Yes	0.9249	0.976146
18	Otu1	Non-essential	Yes	0.944749	0.836696
19	Otu2	Non-essential	Yes	0.854262	0.8604
20	YGL082W	Non-essential	Yes	1.39516	0.846423
21	Rpn11	Essential	No	N/A	

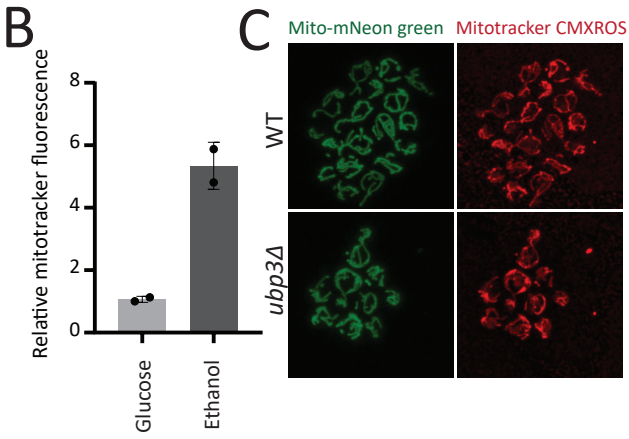

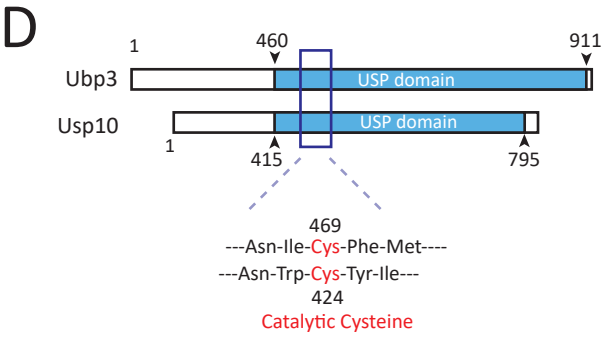

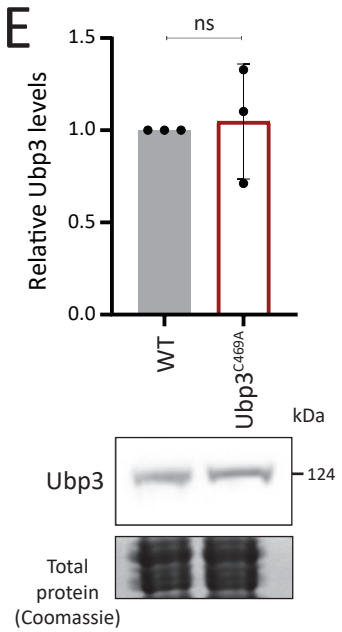

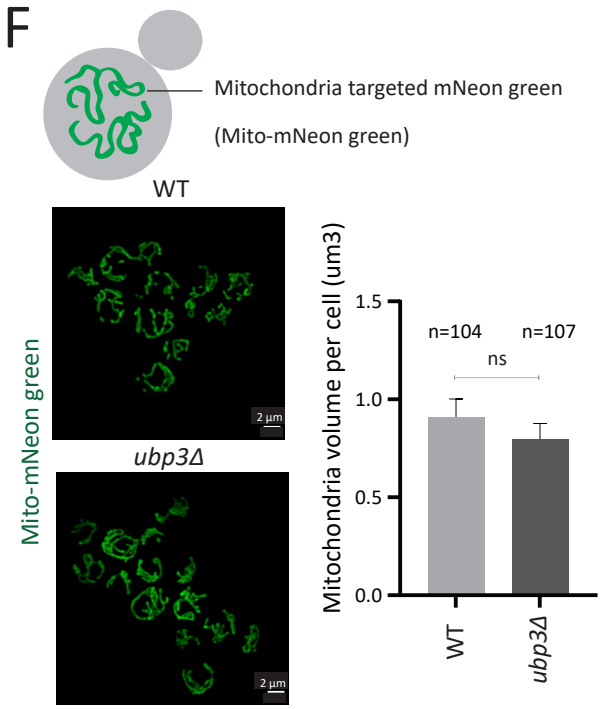

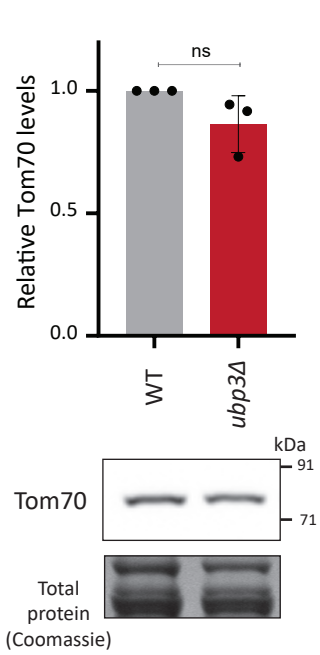

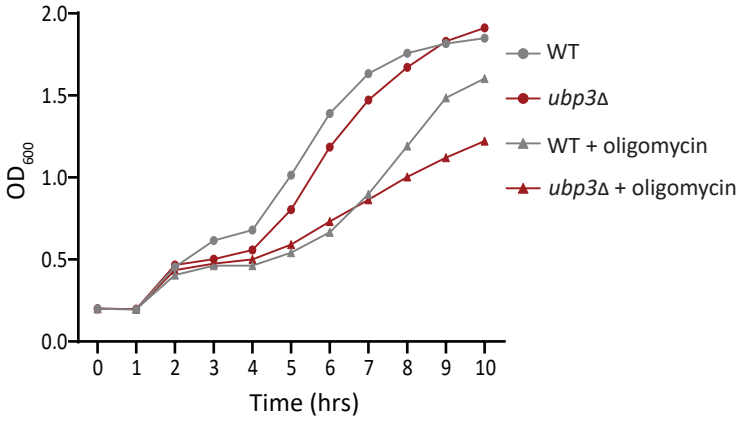

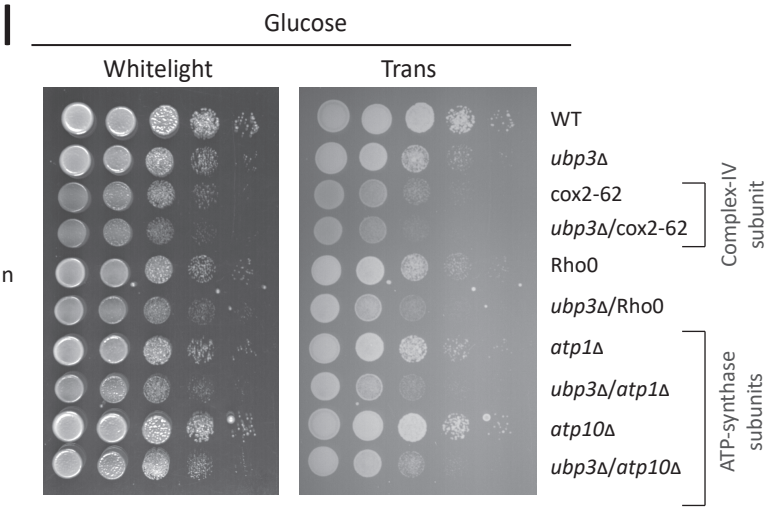

Figure 2-figure supplement 1: Further estimates of glycolytic enzymes and flux

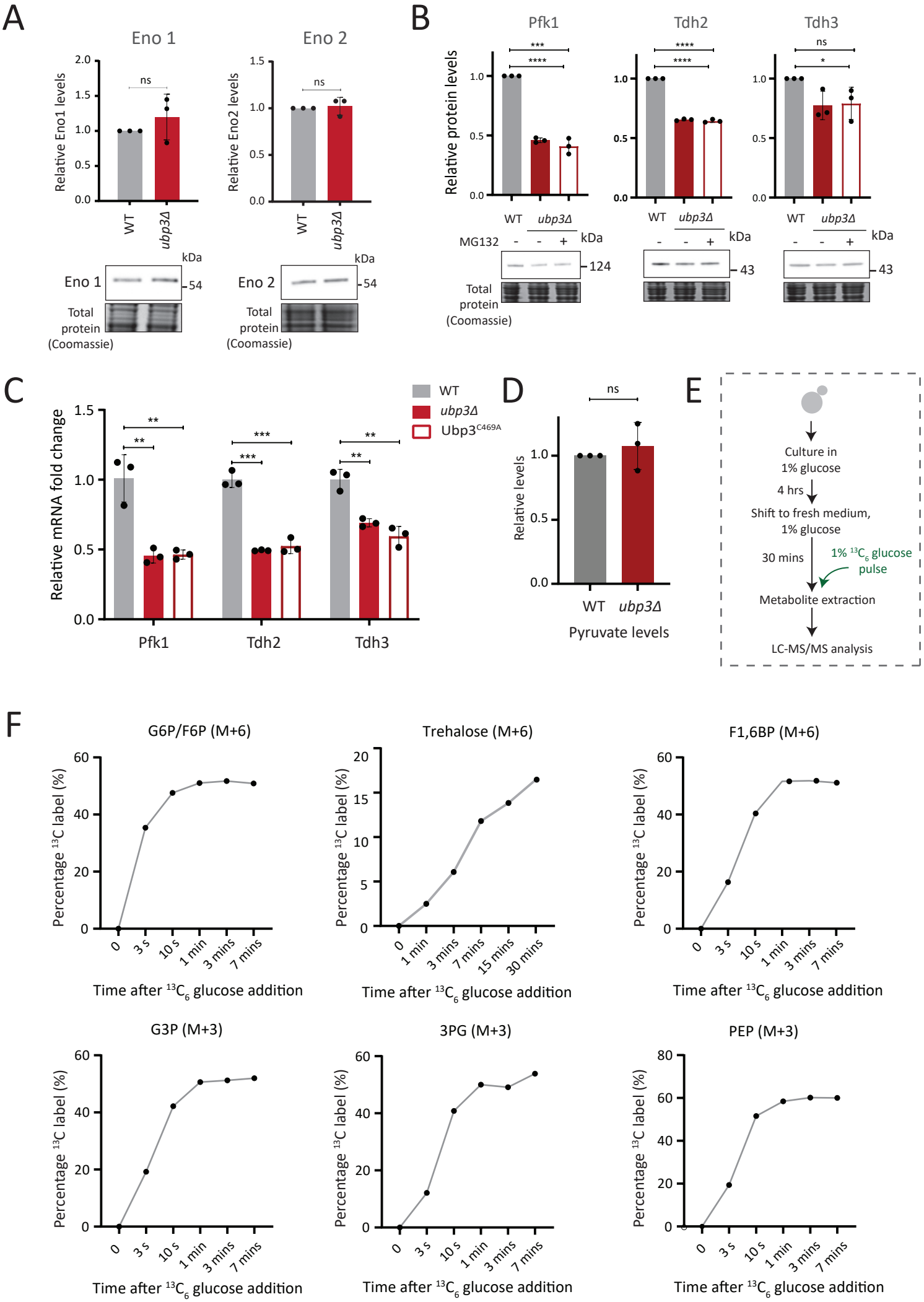

Figure 2-figure supplement 2: Estimation of steady state levels and flux of TCA cycle intermediates

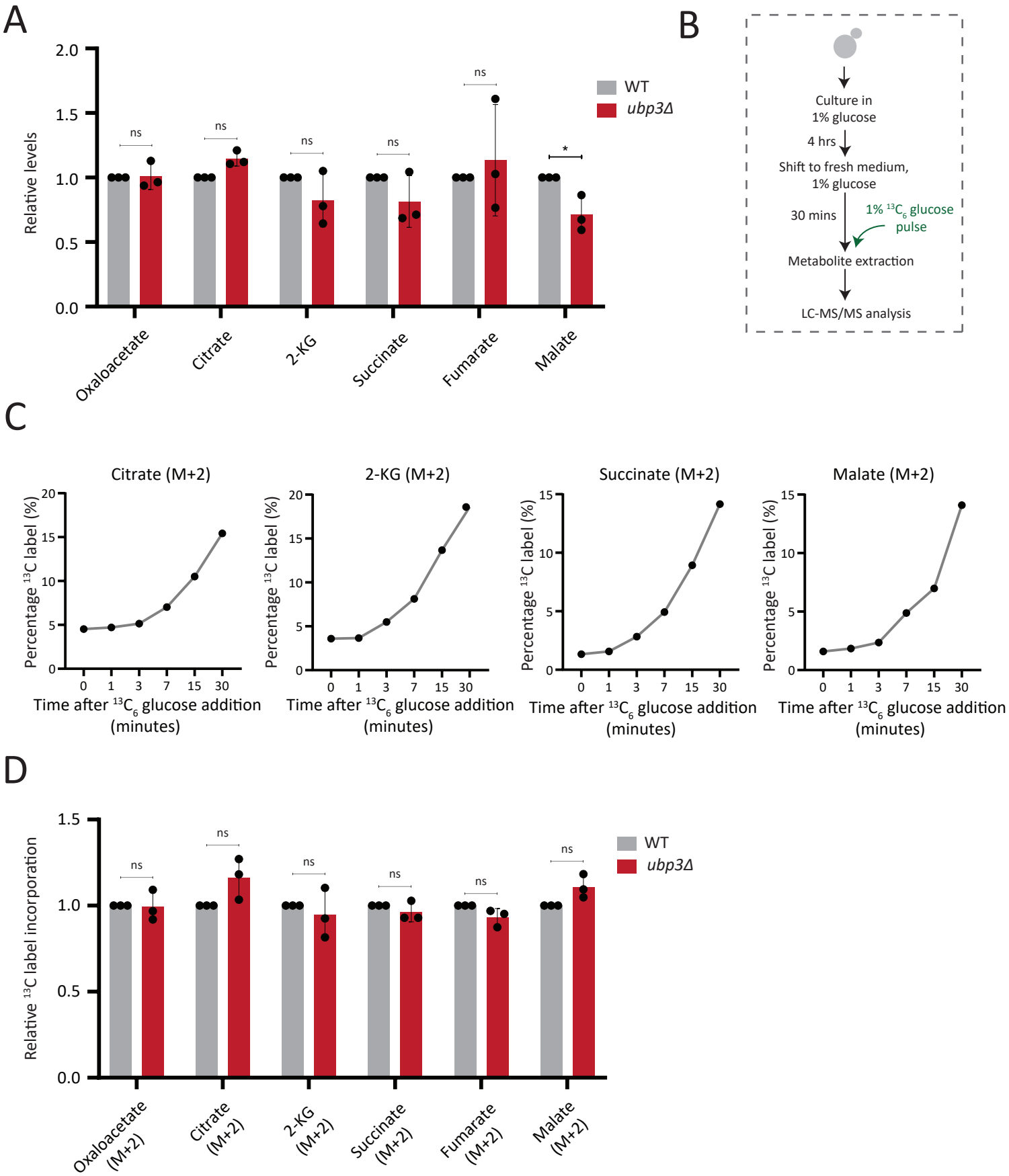

Figure 3-figure supplement 1: Comparisons of phosphate, ethanol and other metabolites in WT, *ubp3Δ* and GAPDH mutants

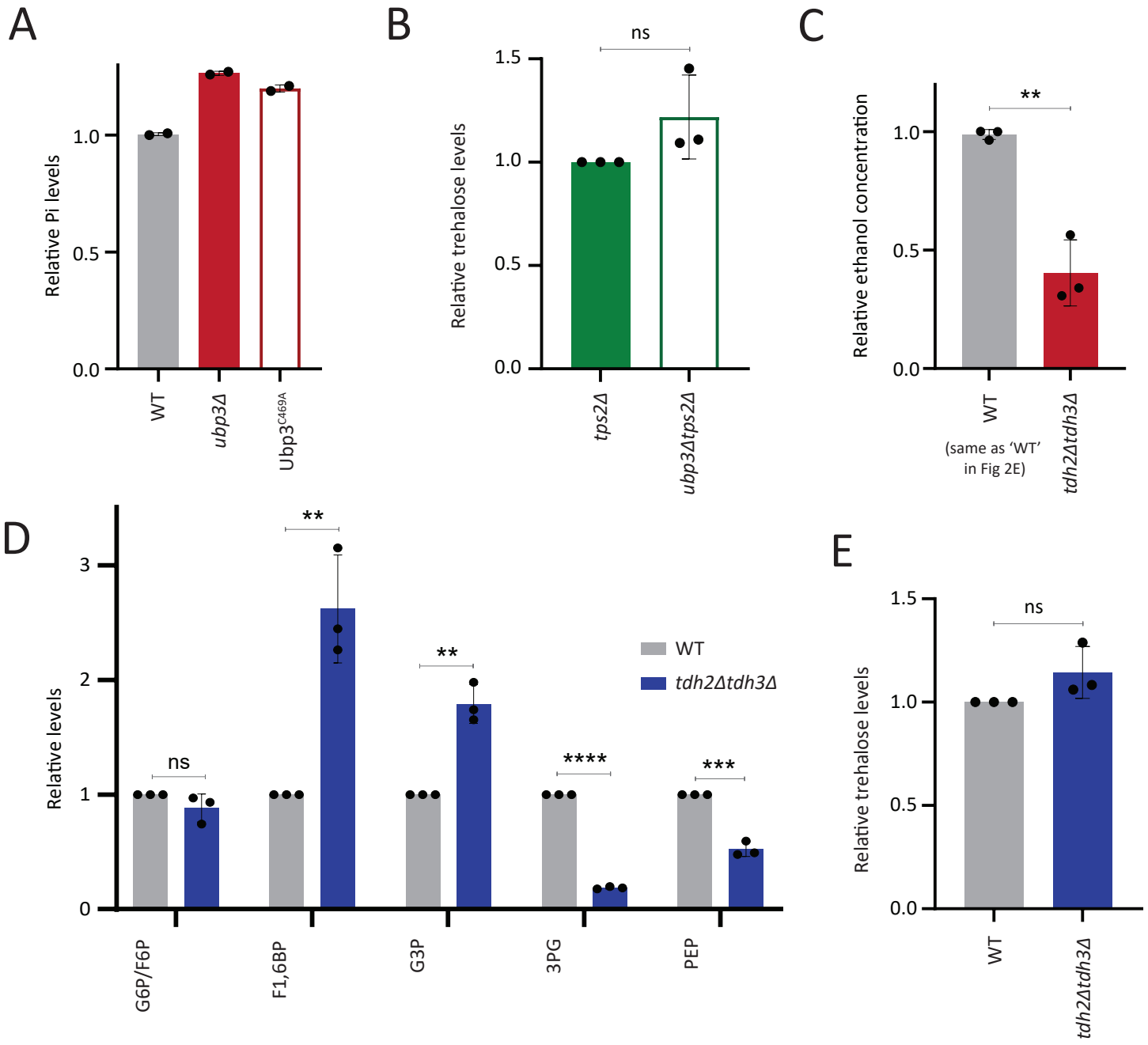

Figure 4-figure supplement 1: Mitochondrial Pi estimation characterizations and correlations of mitochondrial activity with Pi availability

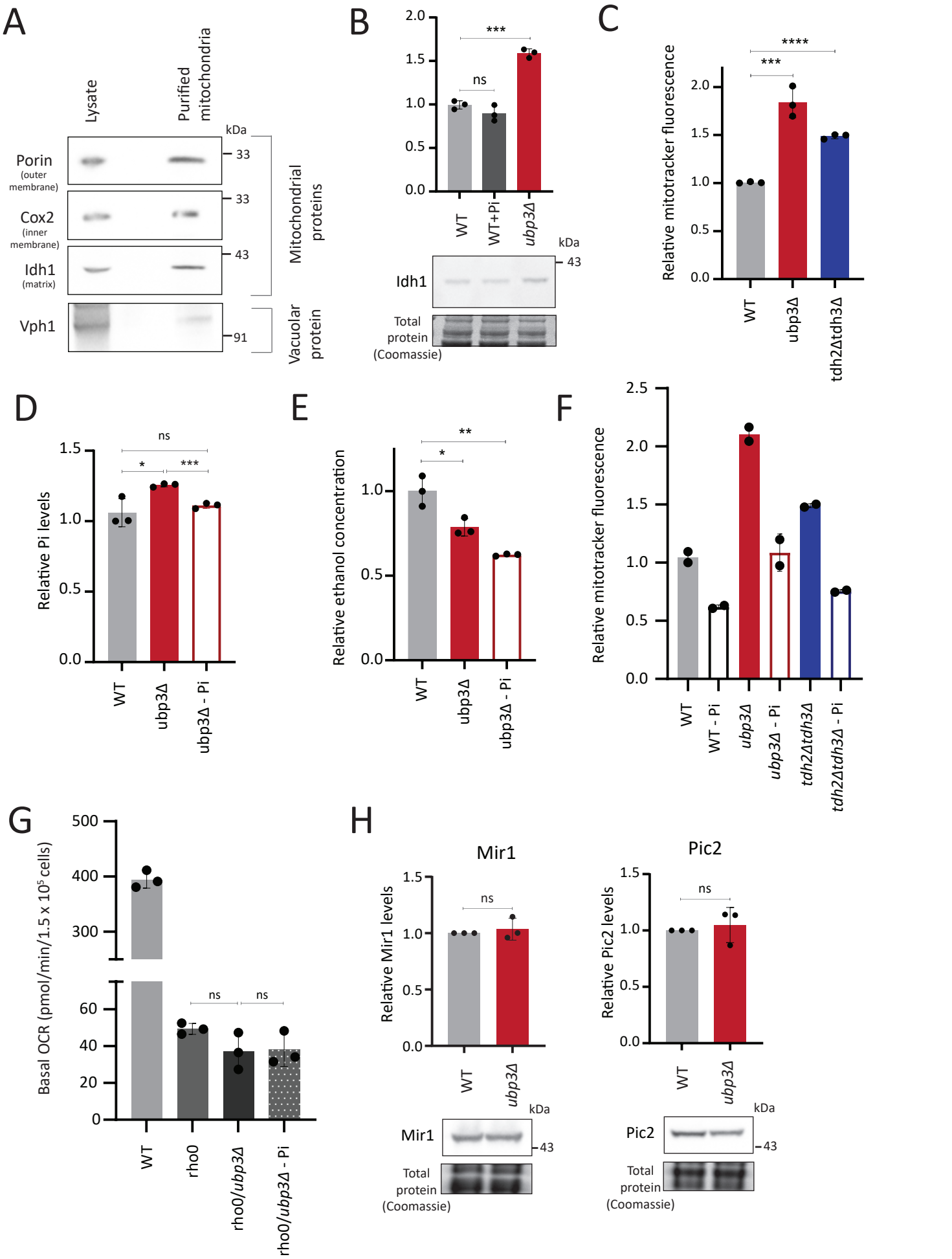
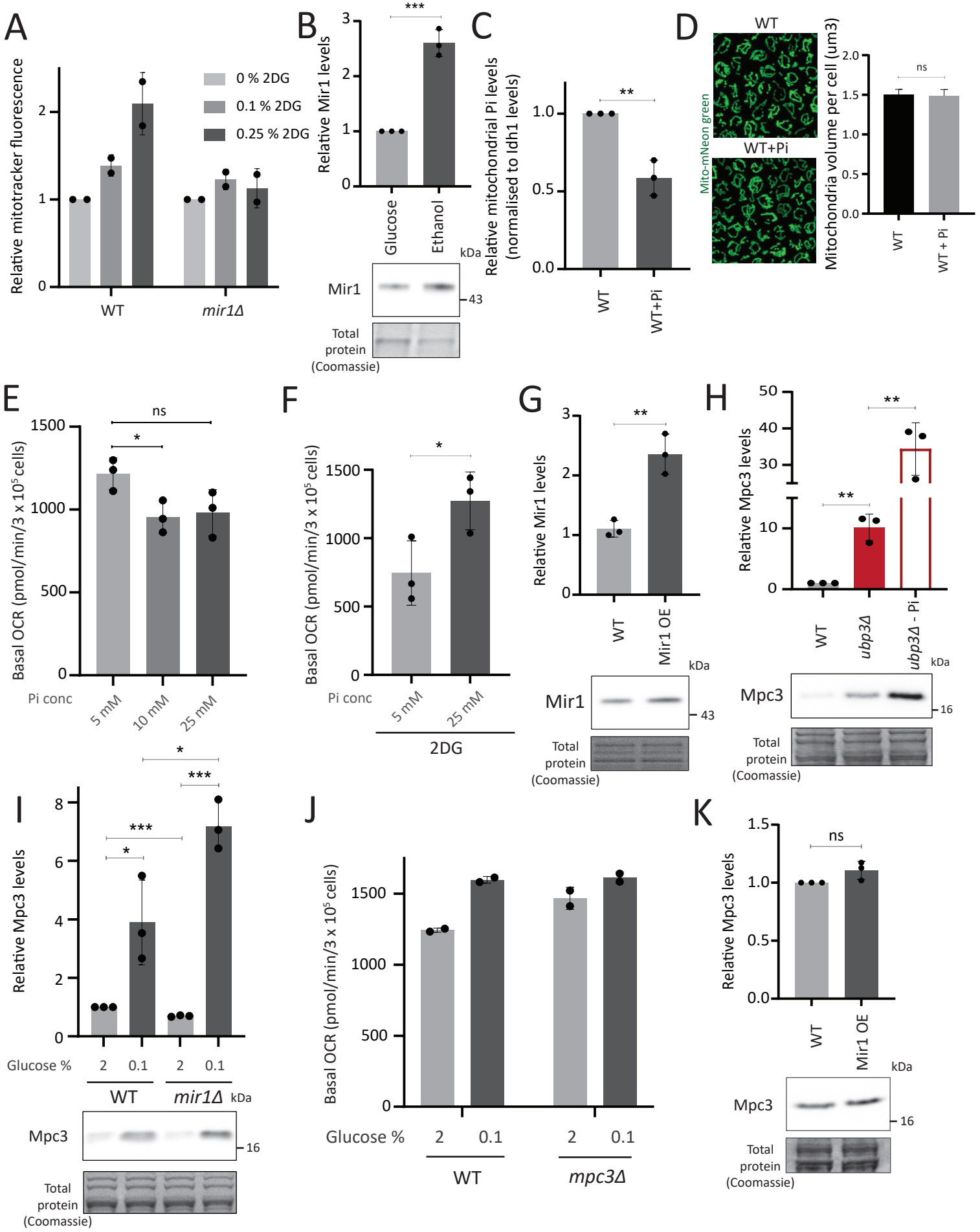
Figure 5-figure supplement 1: Mitochondrial phosphate and pyruvate transport relationships with mitochondrial activity